

1 **Terrestrial responses of low-latitude Asia to the Eocene-**  
2 **Oligocene climate transition revealed by integrated**  
3 **chronostratigraphy**

4  
5  
6  
7  
8 **Yong-Xiang Li<sup>1</sup>, Wenjun Jiao<sup>1</sup>, Zhonghui Liu<sup>2</sup>, Jianhua Jin<sup>3</sup>, Dehai Wang<sup>4</sup>, Yuxin**  
9 **He<sup>5</sup>, and Cheng Quan<sup>6</sup>**

10  
11  
12  
13 <sup>1</sup> State Key Laboratory for Mineral Deposits Research, School of Earth Sciences and  
14 Engineering, Institute of Geophysics and Geodynamics, Nanjing University, Nanjing 210046,  
15 China

16 <sup>2</sup> Department of Earth Sciences, The University of Hong Kong, Hong Kong, China

17 <sup>3</sup> State Key Laboratory of Biocontrol and Guangdong Provincial Key Laboratory of Plant  
18 Resources, School of Life Sciences, Sun Yat-sen University, Guangzhou 510275, China

19 <sup>4</sup> College of Earth Sciences, Jilin University, Changchun 130061, China

20 <sup>5</sup> Department of Earth Sciences, Zhejiang University, Hangzhou, China

21 <sup>6</sup> Research Center of Paleontology and Stratigraphy, Jilin University, Changchun 130026,  
22 China

23  
24  
25  
26 Correspondence to: Yong-Xiang Li (yxli@nju.edu.cn); Cheng Quan (quan@jlu.edu.cn)

## 1 **Abstract**

2 The Paleogene sedimentary records from southern China hold important clues to the impacts  
3 of the Cenozoic climate changes on low-latitudes. However, although there are extensive  
4 Paleogene terrestrial archives and some contain abundant fossils in this region, few are  
5 accurately dated and have a temporal resolution adequate to decipher climate changes. Here  
6 we present a detailed stratigraphic and paleomagnetic study of a fossiliferous late Paleogene  
7 succession in the Maoming Basin, Guangdong Province. The succession consists of oil shale  
8 of the Youganwo Formation (Fm) in the lower part and the overlying sandstone-dominated  
9 Huangniuling Fm in the upper part. Fossil records indicate that the age of the succession  
10 possibly spans from late Eocene to Oligocene. Both the Youganwo Fm and the overlying  
11 Huangniuling Fm exhibit striking sedimentary rhythms, and spectral analysis of the depth  
12 series of magnetic susceptibility of the Youganwo Fm reveals dominant sedimentary cycles at  
13 orbital frequency bands. The transition from the Youganwo oil shale to the overlying  
14 Huangniuling sandstones is conformable and represents a major depositional environmental  
15 change from a lacustrine to a deltaic environment. Integrating the magnetostratigraphic,  
16 lithologic, and fossil data allows establishing a substantially refined chronostratigraphic  
17 framework that places the major depositional environmental change at 33.88 Ma, coinciding  
18 with the Eocene–Oligocene climate transition (EOT) at ~33.7 to ~33.9 Ma. We suggest that  
19 the transition from a lacustrine to deltaic environment in Maoming Basin represents terrestrial  
20 responses to the EOT and indicates prevailing drying conditions in low-latitude regions  
21 during the global cooling at EOT.

22

## 23 **1 Introduction**

24 The late Paleogene witnessed one of the most prominent climatic changes in the Cenozoic, a  
25 transition from greenhouse to icehouse world. The transition is climaxed at the Eocene–  
26 Oligocene boundary when marine sediments registered a large, widespread, and rapid cooling  
27 in oceans (e.g., Zachos et al., 2001; Liu et al., 2009; Bohaty et al., 2012), which was  
28 accompanied by a sudden deepening of the carbonate compensation depth (CCD) by ~1.2 km  
29 (Pälike et al., 2012) in oceans and a severe calamity in the marine community that gave rise to  
30 the largest marine mass extinction since the end of Cretaceous (e.g., Prothero, 1994; Pearson  
31 et al., 2008; Cotton and Pearson, 2011). On land, this transition is expressed as rapid ice sheet  
32 growth over Antarctica (e.g., DeConto and Pollard, 2003; Coxall et al., 2005; Goldner et al.,

1 2014) and large-scale cooling (e.g., Zanzazi et al., 2007; Dupont-Nivet et al., 2007; Hren et al.,  
2 2013). While the transition is widely recognized in the marine realm (Zachos et al., 2001;  
3 Jovane et al., 2006; Liu et al., 2009; Pälike et al., 2012; Westerhold et al., 2014) and is  
4 increasingly well-defined in terrestrial records from the Atlantic region (e.g., Zanzazi et al.,  
5 2007; Hren et al., 2013), its impacts on Asian environment remain poorly understood. This is  
6 largely because the concomitant tectonism, i.e., the Tibetan plateau uplift, and the  
7 development of monsoonal climate may also impose strong influence on Asian environment  
8 (e.g., Dupont-Nivet et al., 2007; Quan et al., 2012, 2014; Wang et al., 2013; Licht et al., 2014,  
9 2015; Shukla et al., 2014).

10 There are numerous basins in southern China that host conspicuous Cenozoic sedimentary  
11 archives documenting the Cenozoic climate changes in the region. The late Paleogene  
12 sedimentary records from this region are of particular interest because they hold clues to the  
13 dramatic shift of climates in low-latitude Asia (Quan et al. 2012; Wang et al., 2013; Licht et  
14 al., 2014, 2015), where the influence of the Tibetan Plateau uplift should be minimal in  
15 comparison to the Asian interior. However, although abundant Paleogene sedimentary  
16 successions were developed here (e.g., Tong et al., 2005; 2013), their age controls are  
17 generally poor. Despite the fact that some successions contain vertebrate and/or plant fossils  
18 (e.g., Tong et al., 2005; 2013), the indicative age ranges of these fossils are often too broad to  
19 date climate changes with satisfactory accuracy and precision.

20 In this paper, we present a detailed stratigraphic and paleomagnetic study on the fossiliferous  
21 Eocene to Oligocene succession in the Maoming Basin of Guangdong Province, southern  
22 China to construct a new chronostratigraphic framework that is based on an integrated litho-,  
23 bio-, magneto-, and cyclostratigraphy. The new chronology not only greatly reduces the  
24 uncertainty but also significantly refines the available fossil-based timescale of the succession.  
25 In particular, the substantially refined chronology permits establishing the link between the  
26 dramatic environmental change in the basin and the global Eocene-Oligocene climatic  
27 transition, and thus provides a critical chronological basis for further detailed examination of  
28 climate changes in this region.

## 29 **2 Geologic setting**

30 The Maoming Basin is an intramontane basin situated in the southwestern part of Guangdong  
31 Province, southern China (Fig. 1). The Cenozoic succession of the basin consists of, from the  
32 bottom to the top, the Shangdong Formation (Fm), Youganwo Fm, Huangniuling Fm,

1 Shangcun Fm, Laohuling Fm, and Gaopengling Fm (BGMRGP, 1988, 1996). Among these  
2 units, the Eocene to Oligocene strata concern the Youganwo Fm and the Huangniuling Fm  
3 (Fig. 2).

4 The Youganwo Fm is characterized by the occurrence of siltstones and shales containing coal  
5 seams in the lower part and the predominant occurrence of oil shales in the upper part (Fig. 2).  
6 The Youganwo Fm contains abundant vertebrate and plant fossils including turtles of  
7 *Anosteira maomingensis*, *Isometremys lacuna* and *Adocus inexpectatus* (Chow and Liu, 1955;  
8 Chow and Yeh, 1962; Claude et al., 2012; Danilov et al., 2013), crocodiles of *Tomistoma*  
9 *petrolica* and Alligatoridae (Yeh, 1958; Li, 1975; Skutschas et al., 2014), fish of *Cyprinus*  
10 *maomingensis* (Liu, 1957), mammals of *Lunania* cf. *L. youngi* (Wang et al., 2007), and wood  
11 of *Bischofia maomingensis* and *Myrtineoxylon maomingensis* (Feng et al., 2012; Oskolski et  
12 al., 2013). The age of the formation is controversial, varying from Eocene to Oligocene (e.g.,  
13 Liu, 1957; Yeh, 1958; Yu and Wu, 1983). A comprehensive review of the fossil records  
14 suggests that the Youganwo Fm was most likely deposited in the late Eocene (Jin, 2008). The  
15 late Eocene age is interpreted to include both Priabonian stage and the Bartonian stage of the  
16 Eocene based on recent advances in understanding fossil mammals of *Lunania*. Although the  
17 systematic position of the genus *Lunania* is still not fully understood, increasing evidence  
18 appears to point its age at Bartonian to Priabonian stage of the Eocene. To date, two species in  
19 total were reported: *Lunania zhoui* from the Yuanqu Basin of central China (Huang, 2002),  
20 and *Lunania youngi* from Yunnan (Chow, 1957; Zong et al., 1996) and Maoming (Wang et al.,  
21 2007) of southern China, respectively. The geological age of *Lunania zhoui* is regarded to be  
22 no earlier than Bartonian and no later than Priabonian (Tong et al., 2005). For the *Lunania*  
23 *youngi* from Yunnan, its age spans from the Bartonian to Priabonian (Li and Ting, 1983;  
24 Russell and Zhai, 1987; Wang, 1992; Qiu and Wang, 2007), the Bartonian (Tong et al., 1995),  
25 the early Late Eocene (Huang and Qi, 1982), or the latest Eocene (Tong et al., 2005; Wang,  
26 1997). Therefore, the late Eocene age of the mammal fossil in Maoming Basin should be  
27 understood as including both the Priabonian stage and the Bartonian stage of the Eocene.

28 The overlying Huangniuling Fm consists mainly of sandstones and siltstones (Fig. 2). The  
29 lower part of the Huangniuling Fm is dominated by massive, pebbly coarse sandstones  
30 interbedded with thinly bedded, grey, silty mudstones. This formation contains plenty of plant  
31 macrofossils such as fruits, leaves, and reproductive remnants (e.g., Feng et al., 2013). The

1 age of the Huangniuling Fm has been ascribed to late Eocene to Oligocene, or even to the  
2 Miocene (Yu and Wu, 1983; Wang et al., 1994; Guo, 2006; Aleksandrova et al., 2012).

3 The areal extent of these two formations and other Cenozoic architectural units in the  
4 Maoming Basin was mapped by Guo (2006) who compiled stratigraphic data from drill cores  
5 and outcrops. Sedimentary facies analyses of these sedimentary units indicate that alluvial fan  
6 and fan delta were initially developed in the north-eastern part of the basin, which gradually  
7 gave rise to lacustrine environment that expanded to the whole basin and alternated with  
8 deltaic environment as lake area waxed and waned (Guo, 2006). Accordingly, successions  
9 that were accumulated in the lacustrine and deltaic environments often exhibit various  
10 subfacies and microfacies. For instance, subfacies/microfacies analysis indicates that the  
11 lower part of the Youganwo Fm was initially formed in a littoral zone to shallow lake  
12 environment that was replaced by a prodelta environment and subsequently by a shallow lake  
13 environment (Guo, 2006). The oil shale dominated upper part of the Youganwo Fm was  
14 deposited mainly in semi-deep or deep lake environments that gave rise to a shallow lake  
15 environment at the uppermost of the Youganwo Fm. The Huangniuling Fm was deposited  
16 predominately in deltaic environments that vary from prodelta, delta front to delta plain  
17 environments (Guo, 2006). The uppermost part of the Huangniuling Fm, which consists of  
18 mainly muddy siltstone and mudstones, was deposited in a prodelta environment that  
19 transitioned to a shallow lake environment where the younger Shangcun Fm was deposited.

20 A magnetostratigraphic study was previously conducted in the Maoming Basin (Wang et al.,  
21 1994). The paleomagnetic data were collected from three different sites, drill cores MR and  
22 MB as well as an outcrop section MS (Fig. 1b), and stratigraphic data from these three sites  
23 were compiled to obtain a composite stratigraphy that comprises the upper part of Youganwo  
24 Fm, Huangniuling Fm, Shangcun Fm, and Laohuling Fm. The age of the composite  
25 stratigraphy was interpreted to span from Chron 18n to Chron 12n (Wang et al., 1994).  
26 However, the magnetostratigraphy of Wang et al (1994) can only be regarded as preliminary  
27 by modern standards because of the following reasons. The mean sampling spacing is large,  
28 ~2.6 m; In addition, changes in sedimentation rates as indirectly reflected by the lithology  
29 were not taken into account. Furthermore, despite that samples of the Huangniuling Fm,  
30 Shangcun Fm, and Laohuling Fm were collected from the same core, i.e., the 874 m long MR  
31 core, samples of the Youganwo Fm were collected from both the MB core (15 samples) and  
32 the MS section (17 samples). The MB core is 567 m long, penetrates the Cenozoic strata, and

1 reaches the Cretaceous rocks. No details were available as to how these 32 samples from two  
2 different sites were integrated to make a composite stratigraphy for the Youganwo Fm,  
3 particularly given that the MB core is relatively condensed and its base reaches the  
4 Cretaceous rocks. In particular, concerning the stratigraphic interval equivalent to that of this  
5 study, i.e., the upper Youganwo Fm and the lower Huangniuling Fm, the sampling spacing  
6 was on average about 6.0 m (Figs 2 and 5 of Wang et al., 1994), which is too large by modern  
7 standards.

### 8 **3 Methods**

9 The study section is well exposed in the cliffs of the now abandoned open mine pit (N21°  
10 42.3', E110° 53.9'), located to the northwest of the Maoming City (Fig. 1). The exposed  
11 section comprises the upper part of the Youganwo Fm and the overlying Huangniuling Fm. In  
12 this study, the upper 31.5 meter of the Youganwo Fm and the basal 30 meter of the  
13 Huangniuling Fm were measured. Major lithological changes in the upper part of the  
14 Huangniuling Fm are noted. To detect subtle changes in lithology of the exposed Youganwo  
15 Fm, magnetic susceptibility (MS) was measured with a hand-held susceptibility meter SM30,  
16 typically at every 10 to 20 cm. Spectral analysis of the depth MS data series was performed  
17 using the technique of Muller and MacDonald (2000) to detect the dominant sedimentary  
18 cycles. The raw MS data series was first linearly interpolated, detrended, and subjected to a  
19 band-pass filter of 1/1000–1/10 cycles/cm. The prepared MS data series in depth domain was  
20 then used to perform fast Fourier transforms (FFTs), yielding a series of spectral peaks. To  
21 identify the statistically significant spectral peaks, noise estimation using Monte Carlo  
22 approach (Mader et al., 2004) was carried out. This approach involves combining FFTs on  
23 1000 randomly generated datasets to produce a 95% confidence curve. Spectral peaks rising  
24 above the confidence curve are considered statistically significant. To further test whether the  
25 dominant sedimentary cycles, as represented by the statistically significant spectral peaks, are  
26 within orbital frequency bands, cycle wavelength ratios (CWRs) of the dominant sedimentary  
27 cycles are examined and compared with the periodicity ratios of orbital cycles following  
28 Fischer (1991).

29 Oriented paleomagnetic samples were collected from the exposed Youganwo Fm and the  
30 lower part of the overlying Huangniuling Fm at a depositional center of the basin where the  
31 gradual transition between the two formations occur (see Section 4.1). For oil shales in the  
32 Youganwo Fm, samples were collected usually every ~30 to 40 cm and, where possible, 2

1 core samples were taken from a stratigraphic level. For the Huangniuling Fm, samples were  
2 mainly collected from the interbedded thin, gray mudstones. A gasoline-powered portable  
3 rock drill was used to collect samples and a Pomery orientation device was used to orient the  
4 samples. Oriented block samples were taken from outcrops where drilling is not possible. A  
5 total of 109 core samples and 66 block samples from 122 stratigraphic levels were collected  
6 from this section.

7 In the laboratory, the samples were trimmed to standard cylindrical paleomagnetic specimens  
8 or cut into 2 cm cubes (8 cm<sup>3</sup>). Anisotropy of magnetic susceptibility (AMS) of all specimens  
9 was measured with a KLY-3 Kappabridge. The specimens were then subjected to progressive  
10 thermal or AF (alternating field) demagnetization. The AF demagnetization was performed  
11 with a Molspin demagnetizer and the thermal demagnetization was conducted with an ASC  
12 TD48 thermal demagnetizer. The remanence of specimens was measured with a three-axis,  
13 2G Enterprise Inc. 755 rock magnetometer. To constrain the magnetic mineralogy, isothermal  
14 remanent magnetization (IRM) acquisition was conducted with an ASC impulse magnetizer  
15 (IM-30) for selected samples. In the IRM acquisition experiments, each sample was  
16 magnetized in a forward field that progressively increases from 20 mT to 1.2 T. The sample  
17 was then progressively demagnetized in a backward field to estimate the coercivity of  
18 magnetic minerals. Between each magnetization/demagnetization treatment, the remanence of  
19 the sample was measured with an AGICO JR6A magnetometer. In addition, selected samples  
20 were subjected to a Lowrie test (Lowrie, 1990) to further constrain the magnetic mineralogy.  
21 In the Lowrie test, the samples were first magnetized sequentially along their Z, Y, and X  
22 axes with fields of 1.2 T, 0.6 T, and 0.125 T, respectively, and the composite IRM was then  
23 thermally demagnetized up to 640 °C. To further aid in magnetic mineralogy determination,  
24 thermal changes of magnetic susceptibility of representative samples from the Youganwo Fm  
25 and the Huangniuling Fm were measured with a MFK Kappabridge equipped with CS4  
26 apparatus. The magnetic susceptibility of the samples was measured while the samples were  
27 heated and cooled between the room temperature and 700 °C in an argon environment. In  
28 addition, Zero-field-cooled (ZFC) and field-cooled (FC) low-temperature measurements were  
29 conducted with a MPMS system at the Paleomagnetism and Geochronology Laboratory,  
30 Chinese Academia of Science. All the demagnetization experiments and remanence  
31 measurements were conducted in a magnetically shielded room (residual field < 300 nT) in  
32 the Paleomagnetism Laboratory of Nanjing University, China.

1 The demagnetization data were analyzed using the principal component analysis technique  
2 (Kirschvink, 1980). The demagnetization data are presented graphically with vector end point  
3 diagrams (Zijderveld, 1967). Software packages Puffinplot (Lurcock and Wilson, 2012) and  
4 PMGSC (by Randy Enkin) were used for paleomagnetic data analysis. The defined polarity  
5 zones, together with constraints from the paleontologic and lithologic data, are compared with  
6 the Geomagnetic Polarity Time Scale (GPTS) of Ogg (2012) to establish a chronologic  
7 framework for the investigated section.

## 8 **4 Results**

### 9 **4.1 Sedimentary rhythms**

10 The lithostratigraphy of the investigated section is summarized in Fig. 2. At distance, the  
11 lithology difference of the Youganwo Fm at the lower part and the Huangniuling Fm at the  
12 upper part of the section is indicated by the distinct color contrast (Fig. 2c-e). The overall  
13 light brownish color in the lower part characterizes the exposed Youganwo Fm, while the  
14 overall pale grey to light yellowish color in the upper part characterizes the overlying  
15 Huangniuling Fm (Fig. 2e). The investigated Youganwo Fm consists predominately of brown  
16 to dark brown oil shales with faint thin laminations. Brown grey to grey mudstone occurs at  
17 the uppermost of the Youganwo Fm. The overlying Huangniuling Fm contains dominantly  
18 massive sandstone and siltstone beds that are interbedded with pale grey to grey thin  
19 mudstones beds.

20 One of the most striking features of the outcrop is the occurrence of sedimentary rhythms,  
21 which are impressively expressed as the repeated occurrence of beds with distinct reddish  
22 color, in both the Youganwo Fm and the Huangniuling Fm (Fig. 2c, e). In the Youganwo Fm,  
23 there are more than a dozen of beds displaying distinct reddish color (Fig. 2a). The  
24 sedimentary rhythm is particularly well expressed between ~11 m and 30 m, where the  
25 average spacing between two neighboring reddish beds is about 1.0 to 1.5 m (Fig. 2a).  
26 Inspection of the beds with reddish color at the outcrop found that the reddish coloration only  
27 occurs at the surface and should represent weathering banding of the beds because the fresh  
28 exposure of these beds does not show reddish color. Despite that the reddish color represents  
29 recent weathering, not the depositional signature, weathering enhanced the expression of  
30 changes in lithology and made the subtle lithological changes more distinctly and  
31 expressively visible on the outcrop. Because the reddish layers correspond to higher magnetic



1 susceptibility (MS) values and less reddish levels display relatively lower MS values, MS data  
2 can facilitate the characterization of sedimentary cycles in the Youganwo Fm. Indeed, our  
3 high-resolution MS data also exhibit meter-scale cyclicity (Fig. 2b). Spectral analysis of the  
4 MS data reveals dominant sedimentary cycles with a cycle wavelength of ~252 cm, 127 to  
5 107 cm, and ~30 cm, respectively (Fig. 3). The 127 to 107 cm cycle and the ~30 cm cycle  
6 have a cycle wavelength ratio of 3.6 to 4.2:1. The ~252 cm cycle and the 127 to 107 cm cycle  
7 have a cycle wavelength ratio of 1.98 to 2.35:1.

8 The contact between the Youganwo Fm and the overlying Huangniuling Fm is sharp at many  
9 locations around the edge of the open mine pit where the siltstone and sandstone dominated  
10 Huangniuling Fm directly sits atop of brown grey to dark grey mudstones of the upper part of  
11 the Youganwo Fm. However, when the contact is traced toward the center of the basin, the  
12 interface between the two formations is represented by a ~ 50 cm thick layer that displays a  
13 continuous, gradual change from brown grey mudstones at the uppermost Youganwo Fm to  
14 pale grey mudstones at the base of the Huangniuling Fm (Fig. 2d). Above the pale grey  
15 mudstone are siltstones and sandstones, exhibiting a coarsening upward trend in grain size.  
16 Further upsection, the siltstones and sandstones are interbedded with thin layers of pale grey  
17 mudstones in the lower part of the Huangniuling Fm.

18 In the Huangniuling Fm, sedimentary rhythms are indicated by repeated occurrence of  
19 distinct red layers. The red layer occurs at the base of the pale grey massive coarse sandstone  
20 and is typically a few centimeters thick. The basal red sandstones are more resistant to  
21 weathering than the rest of the massive sandstones and commonly stick out of the surface of  
22 the outcrop, making the distinct red layers readily recognizable at distance (Fig. 2c). The  
23 thickness of the massive sandstone varies largely from decimeters to meters, occasionally up  
24 to decameters. Above massive sandstones is typically a relatively thinner mudstone bed (Fig.  
25 2c). A red layer, massive sandstones, and a thin mudstone bed appear to form a parasequence  
26 that occurs repeatedly across the Huangniuling Fm (Fig. 2a, b, c). In the lower part of the  
27 Huangniuling Fm, the sandstone and mudstone beds in a parasequence are nearly flat and  
28 extend laterally with uniform thickness for hundreds of meters, and there is a fining-upward  
29 trend within a parasequence. In the upper part of the Huangniuling Fm, lense-shaped  
30 channelized sandstones are occasionally observed. Using the distinct red layer in a  
31 parasequence as a marker bed, we have counted 19 parasequences in the exposed  
32 Huangniuling Fm (Fig. 2a, b).

## 1    **4.2    Rock magnetic data**

### 2    **4.2.1    Anisotropy of magnetic susceptibility (AMS)**

3    The AMS data of the Youganwo samples show predominantly oblate fabrics with the  
4    minimum axes perpendicular to the bedding and the maximum and intermediate axes parallel  
5    or subparallel to the bedding (Fig. 4a,b). The degree of anisotropy ( $P_j$ ) ranges from 1.0 to  
6    1.232 (Fig. 4b). The AMS data of the Huangnuling samples display mainly oblate fabrics (Fig.  
7    4d), but also show a weak prolate fabric with the maximum axes trending SE and the  
8    minimum and intermediate axes girdling along the NE-SW direction (Fig. 4c). In addition, the  
9    degree of anisotropy of the Huangniuling samples is low, varying from 1.0 to 1.089, and  
10    mostly below  $\sim 1.03$  (Fig. 4d).

### 11   **4.2.2    Temperature-dependence magnetic properties and IRM**

12    Thermomagnetic curves of the samples show that all the low-field magnetic susceptibility  
13    values at the end of the experiments are higher than those at the beginning of the experiments,  
14    suggesting that transformation of magnetic mineral phases occurred during heating (Fig. 5a-e).  
15    Because the cooling curves generally show a rapid increase in susceptibility from 580°C to  
16    500°C (Fig. 5a-e), magnetite minerals were probably produced during the experiments,  
17    leading to elevated susceptibility values by the end of the experiments. The mudstone at the  
18    lower part of the Huangniuling Fm (Fig. 5a,b) and the brown grey shale of the uppermost  
19    Youganwo Fm (Fig. 5c) show overall similar features with an increase in magnetic  
20    susceptibility between 450°C and 500°C during heating, whereas the oil shale samples show  
21    an increase in magnetic susceptibility at  $\sim 250^\circ\text{C}$  and another major increase between 400°C  
22    and 450°C (Fig. 5d,e) during heating. For the oil shale samples, the magnetic susceptibility  
23    increase at  $\sim 250^\circ\text{C}$  (Fig. 5d,e) is diagnostic of hexagonal pyrrhotite due to thermally activated  
24    vacancy ordering (Dunlop and Özdemir, 1997), and the subsequent increase in magnetic  
25    susceptibility between 450°C and  $\sim 500^\circ\text{C}$  probably indicates transformation of pyrrhotite to  
26    magnetite during heating (Fig. 5d,e).

27    IRM acquisition of the samples shows that these samples are mostly saturated at fields above  
28    200 mT (Fig. 5f). The demagnetization of IRMs in the backward DC fields suggests that the  
29    coercivity of the magnetic minerals is around 40 mT (Fig. 5f). The ZFC and FC low-  
30    temperature data of the samples show that the Huangniuling mudstone and the brown grey  
31    shale of the uppermost part of the Youganwo Fm exhibit similar features that are

1 characterized by a small difference between the ZFC and FC curves (Fig. 5g, h). In addition,  
2 the Huangniuling mudstone shows a subdued transition at ca. 120 K (marked with an arrow in  
3 Fig. 5g), which may indicate the presence of magnetite (Verwey, 1939; Özdemir et al., 1993).  
4 Thermal demagnetization of the composite IRM of the Huangniuling mudstone and the brown  
5 grey shale of the Youganwo Fm shows that the low coercivity component (0.125 T)  
6 unblocked at 580°C, confirming that magnetite is the major magnetic mineral phase in the  
7 Huangniuling mudstone and the brown grey shale of the uppermost of the Youganwo Fm. For  
8 the Youganwo oil shale, in addition to the presence of pyrrhotite as indicated by the rapid  
9 increase in magnetic susceptibility at ~250°C (Fig. 5d,e), magnetite is present as well, which  
10 is evidenced by the 580°C unblocking temperature of the composite IRM (Fig. 5o). At some  
11 oil shale levels such as around 17.2 m, iron sulphide phases become predominant, which is  
12 indicated by the sharp drop of the composite IRM between 350°C and 400°C (Fig. 5n). ZFC  
13 and FC low-temperature measurements show that there is a marked difference between the  
14 ZFC and FC curves (Fig. 5i, j), indicating the presence of pyrrhotite (Snowball and Torii,  
15 1999). The  $M_r/\chi$  ratio of the Youganwo oil shale is typically around  $0.5 \times 10^3$  to  $1.0 \times 10^3$   
16 A/m, which is low in comparison to the  $\sim 70 \times 10^3$  A/m for greigite (Snowball and Thompson,  
17 1990). Also, greigite tends to display little difference between ZFC and FC curves (Chang et  
18 al., 2007; Roberts et al., 2011). Therefore, greigite may not be present in Youganwo oil shale.  
19 Pyrrhotite is the dominant iron sulphide phases in the Youganwo oil shale and was likely  
20 produced during the oil shale accumulation.

21

### 22 **4.3 Paleomagnetic data**

23 Natural remanent magnetizations (NRMs) of the samples range between  $3 \times 10^{-3}$  and 20  
24 mA/m with the majority being at the orders of  $10^{-2}$  to  $10^{-1}$  mA/m. About half of the specimens  
25 are magnetically unstable, displaying erratic directions upon demagnetization. For the rest of  
26 the samples, the AF demagnetized samples generally show demagnetization trajectories  
27 decaying toward the origin (Fig. 6a, b, c) and the thermally demagnetized samples generally  
28 show relatively stable demagnetization trajectories below 400 °C (Fig. 6d, e, f), above which  
29 erratic directions occur. For most samples, the linear segment of the demagnetization  
30 trajectory with coercivities  $> 15$  mT or with a temperature range from  $\sim 150$  °C to  $\sim 340$ °C or  
31  $380$ °C that decays toward the origin is regarded as a characteristic remanence (ChRM). The  
32 demagnetization data together with the rock magnetic data (Section 4.2.2) suggest that the

1 remanence of the samples mainly resides in magnetite and pyrrhotite becomes the dominant  
2 magnetic mineral phase in the Youganwo oil shale.

3 To obtain reliable estimates of the ChRMs, the following criteria are also used to scrutinize  
4 the data: a) we generally accept ChRMs of higher coercivity/unblocking temperature  
5 component decaying toward the origin with at least four data points; b) ChRMs with a  
6 maximum angular deviation (MAD) greater than  $16^\circ$  are rejected; c) if two samples from the  
7 same stratigraphic level yield similar ChRMs, the sample that has a better definition of the  
8 ChRM is used. Following the above treatments, we obtain reliable paleomagnetic data from  
9 63 stratigraphic levels. Among these data, ChRMs from 46 stratigraphic levels have their  
10 corresponding virtual geomagnetic pole (VGP) within  $45^\circ$  from the mean of VGPs. These 46  
11 ChRMs show both normal and reversed polarities (Fig. 7). A reversal test was performed and  
12 passed at 95% confidence level with class “C” (McFadden and McElhinny, 1990). Therefore,  
13 the quality of the 46 ChRMs is ranked at “A” and the remaining 17 ChRMs are ranked at “B”  
14 in quality. Changes in inclinations and VGP latitudes of these ChRMs with depth are shown  
15 in Fig. 8c, d.

16

## 17 **5 Discussions**

### 18 **5.1 Depositional environment**

19 The history of depositional environmental changes in Maoming Basin was summarized by  
20 Guo (2006). For the investigated section in this study, the upper part of the Youganwo oil  
21 shale was deposited in semi-deep or deep lake environment that gradually transitioned to a  
22 shallow lake environment at the uppermost of the Youganwo Fm (Guo, 2006). The striking  
23 sedimentary rhythms are dominated by 127 to 107 cm cycles and 30 cm cycles, displaying a  
24 cycle wavelength ratio of 3.6 to 4.2:1, which is similar to the periodicity ratio of 4:1 for the  
25 long eccentricity and the short eccentricity cycles. The 252 cm cycle has a cycle wavelength  
26 about 2 times of the 127 to 107 cm cycles, probably representing the harmonics of the 127 to  
27 107 cm cycles. Therefore, the dominant sedimentary cycles are probably in the orbital  
28 frequency bands and the meter-scale cycles may represent the long eccentricity cycle. Since  
29 the Youganwo oil shale was formed in a lacustrine environment (Guo, 2006), such subtle  
30 lithological changes in a repeated fashion as exemplified by the occurrence of the meter-scale  
31 sedimentary cycles were probably related to fluctuating lake levels, which can cause subtle

1 changes in deposition, thus in lithology. Fluctuations of lake level in Maoming Basin may  
2 have been modulated by orbital variations because the dominant sedimentary cycles appear to  
3 be in the orbital frequency bands, probably representing long and short eccentricity cycles.  
4 Orbital variations probably affected moisture conditions in this region, leading to wet/dry  
5 oscillations and thus fluctuations of lake level. Relatively less/more organic matter may have  
6 been accumulated during low/high lake level periods, resulting in subtle cyclic lithological  
7 variations. The subtle lithological changes become expressively displayed as striking  
8 sedimentary cycles on the outcrop upon weathering. The reddish beds probably correspond to  
9 depositions during low lake level periods when relatively less organic matter was  
10 accumulated.

11 The contact between the Youganwo Fm and the Huangniuling Fm shows gradual change from  
12 brown grey mudstones at the uppermost of Youganwo Fm to the pale grey mudstone at the  
13 base of the Huangniuling Fm, which is gradually transitioned to siltstones and further to  
14 sandstones. These features suggest that the deposition was continuous at the study site when  
15 the Maoming Basin experienced the transition from a shallow lacustrine environment, as  
16 represented by the upper part of the Youganwo Fm to a prodelta environment, as represented  
17 by the lower part of the Huangniuling Fm (Guo, 2006), while the lake level was probably  
18 dropping.

19 For the lower part of the Huangniuling Fm, since the sandstone and mudstone beds in a  
20 parasequence are nearly flat and extend laterally with uniform thickness for hundreds of meters,  
21 the lower part of the Huangniuling Fm was likely deposited in a prodelta to delta front or an  
22 interdistributary bay environment. Given the gradual nature of the transition from the  
23 Youganwo Fm to the Huangniuling Fm, the repeated occurrence of the parasequence in the  
24 lower part of the Huangniuling Fm was probably associated with fluctuating lake levels that  
25 may have been forced by orbital variations as well. This notion of orbital forcing is supported  
26 by the persistent pattern of rhythmic occurrence of the parasequences. This notion is also  
27 strengthened by the demonstrated orbital forcing of the deposition in marine (e.g., the  
28 Eocene/Oligocene boundary GSSP section in Italy, Jovane et al., 2006) and lacustrine (e.g.,  
29 the Green River Fm, Meyers, 2008) settings during the similar time interval. For the upper  
30 part of the Huangniuling Fm, the occasional occurrence of lense-shaped channelized  
31 sandstones suggest that delta front to delta plain deposits gradually became dominant in the  
32 upper section.

## 1 **5.2 Definition of magnetozones**

2 Oil shales in the Youganwo Fm exhibit predominantly oblate AMS fabrics (Fig. 4), indicative  
3 of a depositional origin of the fabrics. Silty mudstone layers in the Huangniuling Fm also  
4 show mainly oblate AMS fabrics, and prolate fabrics occur as well, though weak. These  
5 features indicate depositional type of fabrics developed in the presence of currents flowing at  
6 a moderate speed (Tauxe, 1998), which is consistent with a deltaic depositional environment  
7 for the Huangniuling Fm. In addition, reversed polarities are present and a reversal test passed  
8 the confidence criteria (Section 4.3). Taking together, the occurrence of depositional type  
9 fabrics, the presence of reversed polarities, and the passage of a reversal test suggest that the  
10 remanence is likely primary. Therefore, both the VGP latitudes and inclinations are used to  
11 define magnetozones of the investigated sections (Fig. 8e). Also, definition of magnetozones  
12 is primarily based on the “A”-quality ChRM data and the “B”-quality ChRM data are only  
13 used as a second-order constraint for intervals where “A”-quality data are sparse (Fig. 8c, d).  
14 In addition, a polarity zone is defined by at least two consecutive levels of similar polarities.  
15 Changes in inclinations and VGP latitudes with depth are largely in concert, which allows us  
16 to define two reversed polarity zones (R1 and R2) and two main normal polarity zones (N1  
17 and N2) (Fig. 8e). Among these magnetozones N1 and R2 are better defined. N1 is defined  
18 between 32.2 m and 51.0 m, and R2 is defined from 25.0 m to 32.2 m (Fig. 8e). Below 25.0 m  
19 is dominated by the normal polarities except at ~ 10 m where isolated negative inclinations  
20 and VGP latitudes occur (Fig. 8c, d). Although these negative values do not occur  
21 consecutively in depth (Fig. 8c, d), the trend of shift toward negative values in both  
22 inclinations and VGP latitudes is evident and is consistent, suggesting that a reversed polarity  
23 probably exists at ~10 m (Fig. 8e). This possible reversed polarity zone is tentatively defined  
24 between ~11.0 m and ~8.5 m and separates the lower 25 m section into two short normal  
25 polarity zones, N2 and N3 (Fig. 8e).

## 26 **5.3 Major constraints on a geomagnetic polarity timescale (GPTS)**

27 Correlation of these magnetozones to the standard GPTS is not unique due to the lack of  
28 numerical ages serving as anchor points. However, several constraints exist for the  
29 investigated section. When these constraints are used collectively and in conjunction with the  
30 defined magnetozones (Fig. 8e), it is possible to establish a reliable polarity time scale for this  
31 section.

1 The major constraints are as follows. First, the studied oil shales contain abundant vertebrate  
2 and plant fossils (Chow and Liu, 1955; Liu, 1957; Yeh, 1958; Chow and Yeh, 1962; Li, 1975;  
3 Yu and Wu, 1983; Wang et al., 2007; Claude et al., 2012; Feng et al., 2012, 2013). In  
4 particular, the mammal fossil (*Lunania* cf. *L. youngi*) (Wang et al., 2007), which was  
5 unearthed from the studied oil shale of the Youganwo Fm, provides the most definitive  
6 evidence for a late Eocene age (Wang et al., 2007; Jin et al., 2008). Accordingly, the  
7 Youganwo oil shale was formed sometime in the Priabonian stage and/or Bartonian stage of  
8 the Eocene that could span from magnetic Chrons C18r to C13r, i.e., 41 to 34 Ma (Fig. 8f).  
9 Second, the marked difference in lithology of the Youganwo Fm and the Huangniuling Fm  
10 suggests drastic difference in sediment accumulation rates. The sampled Youganwo Fm  
11 consists predominantly of brown oil shales, whereas the overlying Huangniuling Fm  
12 comprises dominantly massive pebbly coarse sandstones and siltstones. Therefore, the  
13 sediment accumulation rates for the Huangniuling Fm were much faster than those for the  
14 Youganwo Fm. In addition, although organic matter and silt content decreases upsection and  
15 grey mudstones occur at the uppermost of the Youganwo Fm, changes in lithology within the  
16 Youganwo Fm are subtle. This suggests that sediment accumulation rates of the studied  
17 Youganwo Fm should not change drastically. Third, the deposition between the Youganwo  
18 and Huangniuling Fms is continuous. The contact between the two formations displays a  
19 continuous, gradual change from brown grey mudstones at the uppermost Youganwo Fm to  
20 pale grey mudstones at the base of the Huangniuling Fm within an interval of ~50 cm. In  
21 addition, siltstones and sandstones overlying the basal pale grey mudstone exhibit a  
22 coarsening upward trend in grain size, indicating a continuous deposition during the transition  
23 from the Youganwo Fm to the Huangniuling Fm. Fourth, the characteristic sedimentary  
24 cycles of the investigated section may also be used as an additional constraint. In fact, the  
25 occurrence of sedimentary cycles is not unique at the studied section. A marine succession of  
26 similar age in Massignano, Italy also displays striking limestone/marl cycles (Jovane et al.,  
27 2006). Cyclic lithologic patterns are also seen in the middle Eocene oil shale-bearing  
28 lacustrine succession in the Mudurnu-Göynük Basin, Turkey (Ocakoglu et al., 2012), the  
29 Eocene oil shale-bearing Green River Formation in the United States (Meyers, 2008), and  
30 other terrestrial records of similar ages in Asia (e.g., Dupont-Nivet et al., 2007; Xiao et al.,  
31 2010). All these lithologic cycles are attributed to orbital forcing and represent orbital cycles  
32 (Jovane et al., 2006; Dupont-Nivet et al., 2007; Meyers, 2008; Xiao et al., 2010; Ocakoglu et  
33 al., 2012). The strong lithologic expression of orbital variations in both marine and terrestrial

1 records, particularly those containing oil shales, from widespread regions at similar ages leads  
2 us to believe that the sedimentary cycles of the studied section probably represent orbital  
3 cycles as well. In particular, spectral analysis of magnetic susceptibility depth series of the  
4 Youganwo Fm reveals dominant sedimentary cycles with a cycle wavelength ratio of  $\sim 4:1$ ,  
5 suggesting that these sedimentary cycles may represent long and short eccentricity cycles.  
6 Therefore, these lithologic cycles can be used as an additional, first-order constraint when  
7 establishing a timescale for the studied section. Based on the definition of the magnetozone  
8 (Fig. 8), there are  $\sim 3.5$  sedimentary cycles in N1. Because a sedimentary cycle in the  
9 Huangniuling Fm is represented by a sequence of red layer, massive sandstone, and a thin  
10 mudstone bed, one red layer marker at 40 m might be unidentified, where the accompanied  
11 thin mudstone bed did occur (Fig. 8). Therefore, there are probably 4 sedimentary cycles in  
12 N1 zone. Similarly, there are  $\sim 3$  sedimentary cycles in R2 zone and  $\sim 8.5$  sedimentary cycles  
13 in N2 zone, respectively (Fig. 8).

#### 14 **5.4 Construction of a geomagnetic polarity timescale (GPTS)**

15 With the aforementioned four constraints, correlations between the four polarity zones (Fig.  
16 8e) and the magnetostratigraphic units C18r to C13r (Fig. 8f) can be examined and unrealistic  
17 correlations can be rejected. Because polarity zones N1 and R2 are better defined than other  
18 two polarity zones, correlation is thus constructed mainly between the N1 and R2 pair and the  
19 consecutive normal and reversed magnetostratigraphic units of the GPTS. To facilitate the analyses, the  
20 N2 zone is also used, but as a secondary constraint, in establishing the correlations.

21 The results of correlations are summarized in Table 1. With the first-order constraint that the  
22 Youganwo oil shales were formed in the late Eocene, i.e., from C18 to C13, six ensembles of  
23 correlations are possible (Table 1). Ensemble 1 correlates N1 and R2 zones with C18n and  
24 C18r, respectively. Ensemble 2 correlates N1 and R2 zones with C17n and C17r, respectively.  
25 Ensemble 3 relates N1 to C16n.2n and R2 to C16r. Ensemble 4 links N1 to C16n.1n, R2 to  
26 C16n.1r, and N2 to C16n.2n. In Ensemble 5, N1 and R2 zones are correlated to C15n and  
27 C15r, respectively. And Ensemble 6 correlates N1 to C13n and R2 to C13r. The quality of  
28 each correlation is assessed by examining whether and to what extent the above four  
29 constraints are met. The one that satisfies most or all of the constraints is preferred and is used  
30 to establish the magnetic polarity timescale for the investigated section. For instance,  
31 Ensemble 1 is rejected because this correlation would force the majority of the Youganwo oil  
32 shale section (N2-N3), where fauna fossils of late Eocene age were discovered, to the middle



1 Eocene (Fig. 8e,f). Ensembles 2 and 3 are rejected on the grounds that the sedimentation rate  
2 for N1 in the coarse sandstones is slower than or similar to that of R2 in the oil shale, which  
3 violates the second constraint. Ensemble 4 is also rejected because the sedimentation rate for  
4 the upper part of the Youganwo Fm (R2) is almost two times that of the lower part of the  
5 Youganwo oil shale, which is incompatible with the subtle compositional change within the  
6 studied Youganwo Fm.

7 For Ensemble 5, assuming that C16n.1r was not captured probably due to its relatively short  
8 duration, N2 zone would correlate to C16n. Such a correlation yields a sedimentation rate of ~  
9 6.37 cm/kyr for N1, ~1.75 cm/ky for R2, and ~1.51 cm/kyr for N2 (Table 1). These  
10 sedimentation rates comply with the constraints specified in Section 5.2. However, the  
11 sedimentation rates of ~1.51 to 1.75 cm/kyr are probably too fast for the investigated oil shale  
12 because oil shale in the Youganwo Fm was formed in a semi-deep to deep lake environment  
13 (Guo, 2006) and the lithology of the investigated interval of the Youganwo Fm is nearly  
14 monotonic, consisting of only oil shale. A pure shale unit represents a condensed time interval  
15 and should be accumulated at very slow rates. Two well-dated organic-rich black shale  
16 intervals in the mid-Cretaceous could serve as useful analog to oil shale of the investigated  
17 section. The well-dated black shale unit at ~120 Ma is about 5 m thick and represents ~1270  
18 kyr (Li et al., 2008), and thus was accumulated at a rate of ~0.39 cm/kyr. Similarly, the  
19 sedimentation rates of the well-dated black shale unit at ~94 Ma (Sageman et al., 2006) are  
20 estimated to be ~0.37 to ~0.50 cm/kyr. In addition, Ensemble 5 correlation would result in a  
21 duration of 295 kyr (C15n) for N1 zone and 411 kyr for R2 zone. Because there are ~4 and ~3  
22 sedimentary cycles in N1 zone and R2 zone, respectively, the sedimentary cycle in N1 zone  
23 and R2 zone would represent a ~74 kyr and ~137 kyr cycle, respectively. The ~137 kyr cycle  
24 in R2 zone could be a result of modulation by short eccentricity of orbital variations. But the  
25 ~70 kyr cycle in N1 zone is not in the frequency band of orbital variations and its origin is  
26 thus difficult to interpret. Therefore, Ensemble 5 is rejected as well.

27 Ensemble 6 satisfies the constraints on sedimentation rates for the Huangniuling Fm and the  
28 Youganwo Fm. Also, the sedimentation rates of 0.42 to 0.56 cm/kyr for the Youganwo Fm  
29 (Table 1) are compatible with those of the well-dated, organic-rich black shales in the mid-  
30 Cretaceous. Furthermore, this correlation would result in durations of N1, R2, and N2 zones  
31 that are largely comparable to those estimated from sedimentary cycles. With Ensemble 6  
32 correlation, N1, R2, and N2 zone would represent ~548 kyr, ~1294 kyr, and ~3334 kyr,

1 respectively. Since N1 zone contains  $\sim 4$  sedimentary cycles (Fig. 8a, b), each cycle would  
2 represent a  $\sim 137$  kyr cycle, which is similar to the short eccentricity cycle E2 (95 to 125 kyr).  
3 Similarly, since there are  $\sim 3$  sedimentary cycles in R2 zone (Fig. 8a, b), each sedimentary  
4 cycle would represent a  $\sim 431$  kyr cycle, which is similar to the long eccentricity cycle E1  
5 (405 to 413 kyr). As an additional check, the duration of the sedimentary cycles within N2  
6 zone is calculated. There are  $\sim 8.5$  sedimentary cycles in N2 zone representing  $\sim 3334$  kyr and  
7 thus each sedimentary cycle has a duration of 392 kyr, which is similar to the periodicity of  
8 long eccentricity cycle E1. Therefore, the sedimentary cycles in the Youganwo Fm are  
9 consistently shown as representing the long eccentricity cycles. It is reasonable that the  
10 sedimentary cycles in N1, i.e., Huangniuling Fm, represent short eccentricity E2 and  
11 sedimentary cycles in R2 represent long eccentricity E1 because the sedimentation rates of the  
12 Huangniuling Fm is much faster than that of the Youganwo Fm and orbital cycles with  
13 shorter durations can be recorded in the Huangniuling Fm. Indeed, among these six ensembles,  
14 only Ensemble 6 can yield periodicities of all the sedimentary cycles, which are from  
15 different parts of the section, in the orbital frequency band within uncertainties (Table 1).  
16 Thus, taking together, Ensemble 6 can satisfy different aspects of major constraints within  
17 uncertainties and thus is acceptable.

18 Analyses of the six possible correlations lead to a conclusion that only Ensemble 6 correlation  
19 offers the most realistic scenario. Therefore, the Ensemble 6 correlation is employed to  
20 establish a chronologic framework for the studied section (Fig. 8e, f). With this chronologic  
21 framework, the transition from the Youganwo Fm to the Huangniuling Fm took place within  
22 magnetochron C13r (Fig. 8). Because the transition is represented by a  $\sim 50$  cm thick,  
23 mudstone-dominated interval and the C13n/C13r boundary (33.705 Ma) occurs at  $\sim 70$  cm  
24 above the top of the transitional interval, the age of the onset of the transition can be  
25 determined by estimating the duration of the  $\sim 1.2$  m thick interval. There are two ways to  
26 estimate the duration of the 1.2 m thick interval. One is to extrapolate the sedimentation rate  
27 of  $\sim 0.56$  cm/kyr for the uppermost part of the Youganwo Fm, i.e., R2 zone. This would lead  
28 to an estimate of  $\sim 210$  kyr and the onset of the transition is then estimated to be at  $\sim 33.915$   
29 Ma. The second approach is to treat the 1.2 m thick interval as the upper part of the long  
30 eccentricity cycle at the uppermost of the Youganwo Fm (Fig. 8a, b). This results in an  
31 estimate of  $\sim 140$  kyr for the 1.2 m thick interval and an onset age of  $\sim 33.845$  Ma. Taking the  
32 average of the above two estimates, we obtain a mean age of 33.88 Ma for the onset of the  
33 transition. In summary, the constructed timescale represents a significantly refined

1 chronology for the Paleogene strata in the Maoming Basin, and provides the tightest possible  
2 constraints on the timing of the onset of the transition from a lacustrine environment to a  
3 deltaic environment in the Maoming Basin.

#### 4 **5.5 Paleoclimatic implications**

5 The rapid transition from a lacustrine environment to a deltaic environment could be related  
6 to global climate change. In the late Paleogene, the Earth's climate underwent a major  
7 transition from greenhouse to icehouse that was climaxed at the Eocene–Oligocene boundary  
8 (Zachos et al., 2001). This climatic transition was accompanied by rapid ice sheet growth on  
9 the Antarctica (e.g., DeConto and Pollard, 2003; Coxall et al., 2005; Goldner et al., 2014) and  
10 was characterized by pronounced global cooling (e.g., Zanazzi et al., 2007; Liu et al., 2009;  
11 Bohaty et al., 2012; Hren et al., 2013). The Eocene–Oligocene transition (EOT) was dated at  
12 33.714 Ma (Jovane et al., 2006) from the marine succession in Massignano, Italy, which is the  
13 Global Stratotype Section and Point (GSSP) for the Eocene–Oligocene boundary. Studies of  
14 the equatorial Pacific records constrain the EOT at ~33.79 Ma (Pälike et al., 2006) or 33.89  
15 Ma (Westerhold et al., 2014). The rapid transition from a lacustrine environment to a deltaic  
16 environment in Maoming Basin is dated at 33.88 Ma, which coincides well with the timing of  
17 the EOT determined from marine records. The close timing suggests strong linkage between  
18 the drastic environmental transition in the Maoming Basin and the EOT (Fig. 8f). The  
19 dramatic shift from a lacustrine to a deltaic environment at the Maoming Basin suggests that  
20 low-latitude Asia likely underwent a transition in regional hydrological cycle from humid to  
21 dry conditions in response to global cooling at the EOT. As dry conditions become prevailed,  
22 lake level likely dropped and lake area became shrunk. The prevailing drying conditions  
23 together with global cooling during EOT probably promoted erosions in upland and supplied  
24 abundant sediments to the shrinking lake, leading to the rapid increase in sediment  
25 accumulation rates after the dramatic environmental change. The dry conditions perhaps  
26 persisted in low-latitude Asia after the dramatic environmental change as the global climate  
27 continued to deteriorate following the rapid, severe, and widespread climatic transition at the  
28 Eocene–Oligocene boundary (Fig. 8f). This persisted dry condition is indicated by the  
29 accumulation of the sandstone-dominated Huangniuling Fm in the Maoming Basin at  
30 relatively increased sedimentation rates. Indeed, similar depositional environmental change  
31 and increase in sedimentation rates between 34.5 Ma and 31 Ma are also observed in Xining  
32 Basin and the E/O climatic transition is considered as a possible cause (Dai et al., 2006).

1 The new, significantly refined chronology also indicates that the striking sedimentary cycles  
2 in both the Youganwo Fm and the Huangniuling Fm likely represent eccentricity cycles. The  
3 recognition of eccentricity signal suggests that sedimentation in the Maoming Basin during  
4 this time interval may have been modulated by orbital variations, probably via lake level  
5 fluctuations at orbital frequency. The occurrence of eccentricity signals in the records is  
6 consistent with the fact the Maoming Basin is situated in the low-latitude areas that are  
7 sensitive to orbital variations at eccentricity frequency bands. Indeed, modulation of orbital  
8 variations on sedimentation appeared to be widespread during this time interval. The long and  
9 short eccentricity signals are also detected from the Eocene/Oligocene Massignano section in  
10 Italy (Jovane et al., 2006). The eccentricity signals are also found in other marine successions  
11 (e.g., Westerhold et al., 2014) and lacustrine deposits (e.g., Meyers, 2008; Okacoğlu et al.,  
12 2012) at the similar ages. Therefore, the drastic environmental change in the Maoming Basin  
13 during EOT represents the terrestrial responses in low-latitude Asia to the EOT that may be  
14 superimposed on the long-term variations at orbital frequency. The investigated section in the  
15 Maoming Basin thus likely faithfully recorded the impacts of the EOT on low-latitude Asia.

16 Another notable feature is the different timings of the major lithologic change the Maoming  
17 terrestrial record and the marine record at Italy. At the GSSP section of Italy, the rapid  
18 lithologic change occurred at early stage of Chron C13r, representing a precursor event of the  
19 EOT (Jovane et al., 2009) (Fig. 8i), while the main lithologic change in the Maoming Basin  
20 took place at late stage of Chron 13r, representing the major event of the EOT (Fig. 8a-f).  
21 This feature may indicate leads/lags of major environmental changes in the terrestrial and  
22 marine realms. The significantly refined chronology of the Maoming record from low-latitude  
23 Asia could potentially help better understand the teleconnection mechanism for the major  
24 global climatic transition across the Eocene-Oligocene boundary.

25

## 26 **6 Conclusions**

27 We have carried out a detailed stratigraphic and paleomagnetic investigation of the upper  
28 Paleogene succession in the Maoming Basin, southern China. The investigated succession  
29 comprises oil shale dominated Youganwo Fm and the overlying sandstone dominated  
30 Huangniuling Fm. Both the Youganwo Fm and the overlying Huangniuling Fm exhibit  
31 striking sedimentary rhythms. The sedimentary rhythms of the Youganwo Fm are well  
32 expressed the high-resolution magnetic susceptibility (MS) data and spectral analysis of the

1 MS depth series reveals that the dominant meter-scale sedimentary cycles are in orbital  
2 frequency bands. The sedimentary rhythms in the Huangniuling Fm are characterized by the  
3 repeated occurrence of a parasequence containing red sandstone layer, massive coarse  
4 sandstones, and a relatively thin mudstone bed. New paleomagnetic results, together with the  
5 lithologic and fossil age data, allow us to establish a magnetostratigraphy for the studied  
6 section that constrains the striking sedimentary cycles of the Youganwo Fm and Huangniuling  
7 Fm to long and short eccentricity cycles, respectively. Taken together, a significantly refined  
8 chronologic framework is established for the investigated succession.

9 The contact between the Youganwo Fm and the Huangniuling Fm is represented by a 50 cm  
10 interval that shows a gradual change from dark grey mudstone at the uppermost of the  
11 Youganwo Fm to the grey mudstone and siltstones with a coarsening upward trend in grain  
12 size at the base of the Huangniuling Fm. This interval represents a major environment change  
13 from a lacustrine to a deltaic environment in the Maoming Basin and its onset is dated at  
14 ~33.88 Ma. The timing of the onset of the dramatic environmental change is in remarkable  
15 similarity with that of the Eocene–Oligocene transition (EOT) that is dated at 33.7 to 33.9 Ma  
16 from various marine records. The synchronicity suggests strong linkage between these two  
17 events and implies that the rapid environmental change in the Maoming Basin most likely  
18 represents terrestrial responses to the global cooling associated with the EOT. This notion is  
19 strengthened by the subsequent occurrence of the persistently prolonged dry conditions, as  
20 represented by the sandstone-dominated Huangniuling Fm, following the rapid environment  
21 change coincident with the EOT. These features are highly compatible with the continued  
22 deteriorating conditions after the EOT.

23 In addition, this study demonstrates that it is possible to construct a refined chronologic  
24 framework for a terrestrial record by integrating multiple constraints synergistically from  
25 magnetostratigraphic, lithologic, biostratigraphic, and perhaps cyclostratigraphic data. For this  
26 study, six possible correlations between magnetozones and the standard geomagnetic polarity  
27 timescale (GPTS) are examined and accepted/rejected using four different types of constraints  
28 (Table 1). The robustness of the accepted correlation is thus dependent on how stringent  
29 and/or reliable these constraints are. In this study, although Ensemble 6 is considered as the  
30 most probable correlation after examining all six possible scenarios, constraints derived from  
31 the currently available data may not be stringent enough for a fully definitive choice of  
32 Ensemble 6. For example, the repeated occurrence of parasequences in the upper part of the

1 Huangniuling Fm has not been quantitatively assessed to show convincingly that those  
2 parasequences represent orbital cycles. Also, the 2-3 times difference in sedimentation rates  
3 of oil shale between Ensembles 5 and 6 may not be sufficiently large enough to differentiate  
4 these two ensembles. Therefore, it would be beneficial to acquire more late Paleogene  
5 terrestrial records from other parts of low-latitude Asia in future studies. It would also be  
6 interesting to test whether the major environmental change in low-latitude Asia truly  
7 coincides with the main EOT event or represents responses to a precursor event of EOT.  
8 Despite the limitations of the present study, the lack of detailed terrestrial records near the  
9 E/O boundary in continental Southeast Asia makes the results of this study an important  
10 contribution to the understanding of the impacts of the major climatic transition at the end of  
11 Eocene on the environment in low-latitude Asia.

12

13

#### 14 **Acknowledgements**

15 This study was supported by the National Natural Science Foundation of China (Nos.  
16 41210001, 41372002, 41274071, 41230208, 41321062, 41528201), the National Basic  
17 Research Program of China (No. 2012CB822000), and the Fundamental Research Funds for  
18 the Central Universities (20620140389). We thank Shipeng Wang for field assistance, Mike  
19 Jackson, Qingsong Liu, and Xiumian Hu for helpful discussions. Bin Wen, Congcong Gai,  
20 and Shuangchi Liu helped with rock magnetic experiments at the Paleomagnetism and  
21 Geochronology Laboratory, CAS. We are grateful to reviewers Alexis Licht, Christian Rolf,  
22 and Luigi Jovane whose comments were helpful in improving the manuscript.

23

## 1 **References**

- 2 Aleksandrova, G. N., Kodrul, T. M., Liu, X. Y., Song, Y. S., and Jin, J. H.: Palynological  
3 characteristics of the upper part of the Youganwo Formation and lower part of the  
4 Huangniuling Formation, Maoming Basin, South China, in: Proceedings of the 2nd Sino-  
5 Russian Seminar on Evolution and Development of Eastern Asia Flora based on  
6 Palaeobotanical Data, 3–15, Guangzhou, China. School of Life Sciences, Sun Yat-sen  
7 University, Guangzhou, China, 2012.
- 8 Bohaty, S. M., Zachos, J. C., and Delaney, L.M.: Foraminiferal Mg/Ca evidence for Southern  
9 Ocean cooling across the Eocene–Oligocene transition, *Earth Planet. Sci. Lett.*, 317–318,  
10 251–261, 2012.
- 11 Bureau of Geology and Mineral Resources of Guangdong Province: Regional Geology of  
12 Guangdong Province, Geological Publishing House, Beijing, 1988 (In Chinese with  
13 English abstract).
- 14 Bureau of Geology and Mineral Resources of Guangdong Province: Stratigraphy (Lithostratic)  
15 of Guangdong Province, China University of Geosciences Press, Wuhan, 1996 (In  
16 Chinese).
- 17 Chang, L., Robert, A. P., Rowan, C. J., Tang, Y., Pruner, P., Chen, Q., and Horng, C. S.:  
18 Low-temperature magnetic properties of greigite ( $\text{Fe}_3\text{S}_4$ ), *Geochem. Geophys. Geosyst.*,  
19 10, Q01Y04, doi:10.1029/2008GC002276, 2007.
- 20 Chow M.C.: On some Eocene and Oligocene mammals from Kwangsi and Yunnan,  
21 *Vertebrata Palasiatica*, 1(3), 201-214, 1957 (in Chinese with English abstract).
- 22 Chow, M. C., and Liu, C. L.: A new anostherine turtle from Maoming, Kwangtung, *Acta*  
23 *Palaeontol. Sin.*, 3 (4), 275–282, 1955 (In Chinese with English abstract).
- 24 Chow, M. C., and Yeh, H. K., A new emydid from the Eocene of Maoming, Kwangtung,  
25 *Vertebrata Palasiatica*, 6 (3), 225–229, 1962 (In Chinese with English abstract).
- 26 Claude, J., Zhang, J. Y., Li, J. J., Mo, J. Y., Kuang, X. W., and Tong, H. Y.: Geoemydid  
27 turtles from the Late Eocene Maoming basin, southern China, *Bull. Soc. géol. France*,  
28 183 (6), 641-651, 2012.

- 1 Coxall, H. K., Wilson, P. A., Pälike, H., Lear, C. H., and Backman, J.: Rapid stepwise onset  
2 of Antarctic glaciation and deeper calcite compensation in the Pacific Ocean, *Nature*,  
3 433, 53–57, 2005.
- 4 Cotton, L. J., and Pearson, P. N.: Extinction of larger benthic foraminifera at the  
5 Eocene/Oligocene boundary, *Palaeogeogr. Palaeoclimatol. Palaeoecol.*, 311, 281–296,  
6 2011.
- 7 Dai, S., Fang, X., Dupont-Nivet, G., Song, C., Gao, J., Krijgsman, W., Langereis, C., and  
8 Zhang, W.: Magnetostratigraphy of Cenozoic sediments from the Xining Basin: Tectonic  
9 implications for the northeastern Tibetan Plateau, *J. Geophys. Res.*, 111, B11102,  
10 doi:10.1029/2005JB004187, 2006.
- 11 Danilov I. G., Syromyatnikova E. V., Skutschas P. P., Kodrul T. M., and Jin J. H.: The first  
12 ‘True’ *Adocus* (Testudines, Adocidae) from the Paleogene of Asia, *J. Vertebr. Paleontol.*,  
13 33(5), 1071–1080, 2013.
- 14 DeConto, R. M., and Pollard, D.: Rapid Cenozoic glaciation of Antarctica induced by  
15 declining atmospheric CO<sub>2</sub>, *Nature*, 421, 245–249, 2003.
- 16 Dunlop, D. J., and Özdemir, Ö.: *Rock Magnetism: Fundamentals and Frontiers*, 573 pp.,  
17 Cambridge Univ. Press, Cambridge, U. K., 1997.
- 18 Dupont-Nivet, G., Krijgsman, W., Langereis, C. G., Abels, H. A., Dai, S., and Fang, X. M.:  
19 Tibetan plateau aridification linked to global cooling at the Eocene – Oligocene  
20 transition, *Nature* 445, 635–638, 2007.
- 21 Feng, X. X., Oskolski, A., and Jin, J.H.: Eocene dicotyledonous wood, *Bischofia*  
22 *maomingensis* sp. nov. from Maoming Basin, South China, *Rev. Palaeobot. Palynology*,  
23 174, 101–105, 2012.
- 24 Feng, X. X., Tang, B., Kodrul, T. M., and Jin, J. H.: Winged fruits and associated leaves of  
25 *Shorea* (Dipterocarpaceae) from the late Eocene of South China and their  
26 phytogeographic and paleoclimatic implications, *Am. J. Bot.*, 100(3), 574 – 581, 2013.
- 27 Fischer, A. G.: Orbital cyclicity in Mesozoic strata, in: *Cycles and Events in Stratigraphy*,  
28 edited by Einsele, G., Ricken, W., and Seilacher, A., Springer-Verlag, Berlin, pp. 48–62,  
29 1991.



- 1 Goldner, A., Herold, N., and Huber, M.: Antarctic glaciation caused ocean circulation  
2 changes at the Eocene–Oligocene transition, *Nature* 511, 574–577,  
3 doi:10.1038/nature13597, 2014.
- 4 Guo, M.: Characteristics and mineralization controlling factors of oil shale in Maoming Basin,  
5 M.Sc. Thesis, Jilin University, 86 pp, 2006.
- 6 Hren, M. T., Sheldon, N. D., Grimes, S. T., Collins, M. E., Hooker, J. J., Bugler, M.,  
7 and Lohmann, K. C.: Terrestrial cooling in Northern Europe during the Eocene–  
8 Oligocene transition, *Proc. Natl. Acad. Sci.*, 110, 7562–7567, 2013.
- 9 Huang, X. S.: New emorpid (Mammalia, Perissodactyla) remains from the middle Eocene of  
10 Yuanqu Basin, *Vertebrata Palasiatica*, 40(4), 286–290, 2002 (in Chinese with English  
11 abstract).
- 12 Huang, X., and Qi, T.: Notes on Late Eocene Tapiroids from the Lunan Basin, eastern  
13 Yunnan, *Vertebrata Palasiatica*, 20(4): 315–326, 1982 (in Chinese with English abstract)
- 14 Jelinek, V.: Characterization of the magnetic fabrics of rocks, *Tectonophysics*, 79, 63– 67,  
15 1981.
- 16 Jin, J. H.: On the age of the Youganwo Formation in the Maoming Basin, Guangdong  
17 Province, *J. Stratigr.*, 32 (1), 47–50, 2008 (In Chinese with English abstract).
- 18 Jovane, L., Florindo, F., Sprovieri, M., and Pälike, H.: Astronomic calibration of the late  
19 Eocene/early Oligocene Massignano section (central Italy), *Geochem. Geophys. Geosyst.*  
20 7, Q07012, doi:10.1029/2005GC001195, 2006.
- 21 Jovane, L., Coccioni, R., Marsili, A., Acton, G.: The late Eocene greenhouse-icehouse  
22 transition: observations from the Massignano global stratotype section and point (GSSP),  
23 *Geol. Soc. Am., Special Paper*, 452, 149–168, 2009.
- 24 Kirschvink, J. L.: The least-squares line and plane and the analysis of paleomagnetic data,  
25 *Geophys. J. Roy. Astron. Soc.*, 62, 699–718, doi: 10.1111/j.1365-246X.1980.tb02601.x.,  
26 1980.
- 27 Li, C., and Ting, S.: The Paleogene mammals of China, *Bulletin of Carnegie Museum of*  
28 *Natural History*, 21, 1–93, 1983 (in Chinese with English abstract).
- 29 Li, J. L.: New materials of *Tomistoma petrolica* Yeh from Maoming, Guangdong, *Vertebrata*  
30 *Palasiatica*, 13 (3), 190–194, 1975 (In Chinese).

- 1 Li, Y. X., Bralower, T. J., Montanez, I. P., Osleger, D. A., Arthur, M. A., Bice, D. M., Herbert,  
2 T. D., Erba, E., and Premoli-Silva, I.: Toward an orbital chronology for the early Aptian  
3 Oceanic Anoxic Event 1a (OAE1a, ~120 Ma), *Earth Planet. Sci. Lett.*, 271, 88–100.  
4 doi:10.1016/j.epsl.2008.03.055, 2008.
- 5 Licht, A. van Cappelle, M., Abels, H. A., Ladant, J.-B., Trabucho-Alexandre, J., and France-  
6 Lanord, C.: Asian monsoons in a late Eocene greenhouse world, *Nature*, 513, 501–506.  
7 doi:10.1038/nature13704, 2014.
- 8 Licht, A., Boura, A., De Franceschi, D., Utescher, T., Sein, C., and Jaeger, J.-J.: Late middle  
9 Eocene fossil wood of Myanmar: Implications for the landscape and the climate of the  
10 Eocene Bengal Bay, *Rev. Palaeobot. Palynol.*, 216, 44–54, 2015.
- 11 Liu, X. T.: A new fossil cyprinid fish from Maoming, Kwangtung, *Vertebrata Palasiatica*, 1  
12 (2), 151–153, 1957 (In Chinese with English abstract).
- 13 Liu, Z. H., Pagani, M., Zinniker, D., DeConto, R., Huber, M., Brinkhuis, H., Shah, S. R.,  
14 Leckie, R. M., and Pearson, A.: Global cooling during the Eocene–Oligocene climate  
15 transition, *Science*, 323, 1187–1190, 2009.
- 16 Lowrie, W.: Identification of ferromagnetic minerals in a rock by coercivity and unblocking  
17 temperature properties, *Geophys. Res. Lett.*, 17, 159–162, 1990.
- 18 Lurcock, P. C., and Wilson, G. S.: PuffinPlot: A versatile, user-friendly program for  
19 paleomagnetic analysis, *Geochem. Geophys. Geosyst.* 13, Q06Z45,  
20 doi:10.1029/2012GC004098, 2012.
- 21 Mader, D., Cleaveland, L., Bice, D., Montanari, A., and Koeberl, C.: High-resolution  
22 cyclostratigraphic analysis of multiple climate proxies from a short Langhian pelagic  
23 succession in the Conero Riveiera, Ancona (Italy), *Paleogeogr. Paleoclimatol. Paleoecol.*,  
24 211, 325–344, 2004.
- 25 McFadden, P.L., and McElhinny, M.W.: Classification of the reversal test in  
26 palaeomagnetism, *Geophys. J. Int.*, 103, 725–729, 1990.
- 27 Meyers, S. R.: Resolving Milankovitchian controversies: The Triassic Latemar Limestone and  
28 the Eocene Green River Formation, *Geology*, 36, 319–322, doi: 10.1130/G24423A.1,  
29 2008.

- 1 Muller, R. A., and MacDonald, J. G.: Ice ages and astronomical causes: Data, spectral  
2 analysis, and mechanisms. Springer Praxis, Berlin, 2000.
- 3 Oçakoğlu, F., Açıkalın, S., Yılmaz, I. Ö., Safak, Ü., and Gökçeoğlu, C.: Evidence of orbital  
4 forcing in lake-level fluctuations in the Middle Eocene oil shale-bearing lacustrine  
5 successions in the Mudurnu-Göynük Basin, NW Anatolia (Turkey), *J. Asian Earth Sci.*,  
6 56, 54–71, 2012.
- 7 Ogg, J. G.: Chapter 5: Geomagnetic Polarity Time Scale, in: *The Geologic Time Scale 2012*,  
8 edited by Gradstein, F.M., Ogg, J.G., Schmitz, M.D., and Ogg, G.M., Elsevier,  
9 Amsterdam, 85–113, 2012.
- 10 Oskolski A. A., Feng X. X., and Jin J. H.: Myrtineoxylon gen. nov.: The first fossil wood  
11 record of the tribe Myrteae (Myrtaceae) in eastern Asia, *Taxon*, 62 (4), 771–778, 2013.
- 12 Özdemir, Ö., Dunlop, D. J., and Moskowitz, B. M.: The effect of oxidation on the Verwey  
13 transition in magnetite, *Geophys. Res. Lett.*, 20, 1671-1674, doi:10.1029/93/GL01483,  
14 1993.
- 15 Pälike, H., Norris, R. D., Herrle, J. O., Wilson, P. A., Coxall, H. K., Lear, C. H., Shackleton,  
16 N. J., Tripathi, A. K., and Wade, B. S.: The Heartbeat of the Oligocene Climate System,  
17 *Science*, 314, 1894–1898, doi:10.1126/science.1133822, 2006.
- 18 Pälike, H., Lyle, M. W., Nishi, H., Raffi, I., Ridgwell, A., Gamage, K., Klaus, A., Acton, G.,  
19 Anderson, L., Backman, J., Baldauf, J., Beltran, C., Bohaty, S. M., Bown, P., Busch, W.,  
20 Channell, J. E. T., Chun, C. O. J., Delaney, M., Dewangan, P., Dunkley Jones, T., Edgar,  
21 K. M., Evans, H., Fitch, P., Foster, G. L., Gussone, N., Hasegawa, H., Hathorne, E. C.,  
22 Hayashi, H., Herrle, J. O., Holbourn, A., Hovan, S., Hyeong, K., Iijima, K., Ito, T.,  
23 Kamikuri, S.-I., Kimoto, K., Kuroda, J., Leon-Rodriguez, L., Malinverno, A., Moore Jr,  
24 T. C., Murphy, B. H., Murphy, D. P., Nakamura, H., Ogane, K., Ohneiser, C., Richter, C.,  
25 Robinson, R., Rohling, E. J., Romero, O., Sawada, K., Scher, H., Schneider, L., Sluijs,  
26 A., Takata, H., Tian, J., Tsujimoto, A., Wade, B. S., Westerhold, T., Wilkens, R.,  
27 Williams, T., Wilson, P. A., Yamamoto, Y., Yamamoto, S., Yamazaki, T., and Zeebe, R.  
28 E.: A Cenozoic record of the equatorial Pacific carbonate compensation depth, *Nature*,  
29 488, 609–614, doi:10.1038/nature11360, 2012.

- 1 Pearson, P. N., McMillan, I. K., Wade, B. S., Dunkley Jones, T., Coxall, H. K., Bown, P. R.,  
2 and Lear, C.H.: Extinction and environmental change across the Eocene–Oligocene  
3 boundary in Tanzania, *Geology*, 36, 179–182, 2008.
- 4 Prothero, D. R.: The late Eocene-Oligocene extinctions, *Annu. Rev. Earth Planet. Sci.*, 22,  
5 145-165, 1994.
- 6 Qiu, Z. X., and Wang, B.: Paraceratheres fossils of China, *Palaeontologica Sinica, New Ser. C*,  
7 29,1-188, 2007 (in Chinese with English abstract).
- 8 Quan, C., Liu, Z. H., Utescher, T., Jin, J. H., Shu, J. W., Li, Y. X., and Liu, Y.-S. C:  
9 Revisiting the Paleogene climate pattern of East Asia: A synthetic review, *Earth-Sci.*  
10 *Rev.*, 139, 213–230, 2014.
- 11 Quan, C., Liu, Y.-S. C., and Utescher, T.: Eocene monsoon prevalence over China: a  
12 paleobotanical perspective, *Palaeogeogr. Palaeoclimatol. Palaeoecol.*, 365–366, 302–311,  
13 2012.
- 14 Roberts, A. P., Chang, L., Rowan, C. J., Horng, C.-S., and Florindo, F.: Magnetic properties  
15 of sedimentary greigite (Fe<sub>3</sub>S<sub>4</sub>): An update, *Rev. Geophys.*, 49, RG1002,  
16 doi:10.1029/2010RG000336, 2011.
- 17 Russell, D. E., and Zhai R. J.: The Paleogene of Asia: mammals and stratigraphy, *Memoires*  
18 *du Museum National d'Histoire Naturelle*, 52, 1-490, 1987.
- 19 Sageman, B. B., Meyers, S. R., and Arthur, M. A.: Orbital time scale and new C-isotope  
20 record for Cenomanian-Turonian boundary stratotype, *Geology*, 34, 125–128,  
21 doi:10.1130/G22074.1, 2006.
- 22 Shukla, A, Mehrotra, R. C., Spicer, R. A, Spicer, T. E. V., and Kumara, M.: Cool equatorial  
23 terrestrial temperatures and the South Asian monsoon in the Early Eocene: Evidence  
24 from the Gurha Mine, Rajasthan, India, *Palaeogeogr. Palaeoclimatol. Palaeoecol.*, 412,  
25 187–198, 2014.
- 26 Skutschas P. P., Danilov I. G., Kodrul T. M., and Jin J. H.: The First Discovery of an  
27 Alligatorid (Crocodylia, Alligatoroidea, Alligatoridae) in the Eocene of China, *J. Vertebr.*  
28 *Paleontol.*, 34(2), 471–476, 2014.
- 29 Snowball, I., and Thompson, R.: A stable chemical remanence in Holocene sediments. *J.*  
30 *Geophys. Res.*, 95, 4471-4479, 1990.

- 1 Snowball, I. F., and Torii, M.: Incidence and significance of magnetic iron sulphides in  
2 Quaternary sediments and soils, in: Quaternary Climates, Environments and Magnetism,  
3 edited by Maher, B. A., and Thompson, R., pp. 199-230, Cambridge Univ. Press,  
4 Cambridge, U.K., doi:10.1017/CBO9780511535635.009, 1999
- 5 Tauxe, L.: Paleomagnetic principles and practice, 301 pp., Kluwer Academic Publisher, 1998.
- 6 Tong, Y., Zheng, S., and Qiu, Z.: Cenozoic mammal ages of China, *Verterbrata Palasiatica*,  
7 33(4), 290-314, 1995 (in Chinese with English abstract).
- 8 Tong, Y. S., Li, Q., and Wang, Y. Q.: A brief introduction to recent advance in the Paleogene  
9 studies, *J. Stratigr.*, 29 (2), 109-133, 2005 (In Chinese with English abstract).
- 10 Tong, Y. S., Li, Q., and Wang, Y. Q.: An introduction to recent advance in the study of the  
11 continental Early Paleogene stages in China, *J.Stratigr.*, 37 (4), 428-440, 2013 (In  
12 Chinese with English abstract).
- 13 Verwey, E. J. W: Electronic conduction of magnetite (Fe<sub>3</sub>O<sub>4</sub>) and its transition point at low  
14 temperatures, *Nature*, 144, 327-328, doi:10.1038/144327b0, 1939
- 15 Wang B.: The Chinese Oligocene: A preliminary review of mammalian localities and local  
16 faunas, in: Eocene-Oligocene Climatic and Biotic Evolution, edited by Prothero D.R.,  
17 and Berggren W. A., Princeton, Princeton University Press, 529-547, 1992 (in Chinese  
18 with English abstract).
- 19 Wang B.: Problems and recent advances in the division of the continental Oligocene,  
20 *Verterbrata Palasiatica*, 21(2), 81-90, 1997 (in Chinese with English summary).
- 21 Wang, D., Lu, S., Han, S., Sun, X., and Quan, C.: Eocene prevalence of monsoon-like climate  
22 over eastern China reflected by hydrological dynamics, *J. Asian Earth Sci.*, 62, 776–787,  
23 2013.
- 24 Wang, J. D., Li, H. M., Zhu, Z. Y., Seguin, M. K., Yang, J. F., and Zhang, G. M.:  
25 Magnetostratigraphy of Tertiary rocks from Maoming Basin, Guangdong Province,  
26 China, *Chinese J. Geochem.*, 13, 165-175, 1994.
- 27 Wang, Y. Y., Zhang, Z. H., and Jin, J. H.: Discovery of Eocene fossil mammal from  
28 Maoming Basin, Guangdong, *Acta Scientiarum Naturalium Universitatis Sunyatseni*, 46  
29 (3), 131-133, 2007 (In Chinese with English abstract).

- 1 Westerhold, T, Röhl, U., Pälike, H., Wilkens, R., Wilson, P.A., and Acton, G.: Orbitally tuned  
2 timescale and astronomical forcing in the middle Eocene to early Oligocene, *Clim. Past*,  
3 10, 955–973, doi:10.5194/cp-10-955-2014, 2014.
- 4 Xiao, G. Q., Abels, H. A., Yao, Z. Q., Dupont-Nivet, G., and Hilgen, F. J.: Asian aridification  
5 linked to the first step of the Eocene-Oligocene climate Transition (EOT) in obliquity-  
6 dominated terrestrial records (Xining Basin, China), *Clim. Past*, 6, 501–513,  
7 doi:10.5194/cp-6-501-2010, 2010.
- 8 Yeh, H. K.: A new crocodile from Maoming, Kwangtung, *Vertebrata Palasiatica*, 2 (4), 237–  
9 242, 1958 (In Chinese with English abstract).
- 10 Yu, J. F., and Wu, Z. J.: Spore-pollen assemblage of Mao 5 well of Maoming Basin,  
11 Guangdong and its geological age, *J. Stratigr.*, 7 (2), 112-118, 1983 (In Chinese).
- 12 Zachos, J. C., Pagani, M., Sloan, L., Thomas, E., and Billups, K.: Trends, rhythms, and  
13 aberrations in global climate 65 Ma to present, *Science*, 292, 686–693, 2001.
- 14 Zanzazi, A., Kohn, M. J., MacFadden, B. J., and Terry, D. O. Jr.: Large temperature drop  
15 across the Eocene–Oligocene transition in central North America, *Nature*, 445, 639–642,  
16 2007.
- 17 Zijderveld, J. D. A.: A. C. demagnetization of rocks: analysis of results, in: *Methods in*  
18 *Palaeomagnetism*, pp. 254–286, edited by D.W. Collinson, K.M. Creer and S.K.  
19 Runcorn, Elsevier, Amsterdam, 1967.
- 20 Zong G.: *Cenozoic Mammals and Environment of Hengduan Mountains Region, China*  
21 *Ocean Press, Beijing*, 279, 1996 (in Chinese with English abstract).
- 22

1 **Table 1** Correlations of magnetozones with Chrons C18 to C13 of the geomagnetic polarity  
2 time scale (GPTS).

3

4 Note:

5 \*, N1 is defined from 32.2 to 51.0 m and contains ~ 4 sedimentary cycles; R2 is defined from  
6 25.0 to 32.2 m and contains ~3 sedimentary cycles; N2 is defined from 11.0 to 25.0 m and  
7 contains ~8.5 sedimentary cycles. Bold (regular) fonts indicate normal (reversed) polarity  
8 zones/chrons; The two numbers in each cell are sedimentation rate in cm/kyr and the  
9 periodicity of the sedimentary cycle (in kyr) calculated based on the correlation. For example,  
10 1.23, 382 in the very first cell indicate that the sedimentation rate is 1.23 cm/kyr and the  
11 sedimentary cycle represents 382 kyr based on Correlation 1. "-" denotes "not applicable"; "x"  
12 indicates that the correlation is unrealistic and is rejected. "√" indicates acceptable  
13 correlations; a-e provide brief comments on why a correlation is rejected or accepted. a, the  
14 correlation would place the majority of the Youganwo Fm, i.e., N2-N3, to the middle Eocene;  
15 b, the correlation would result in sedimentation rates in R2, i.e., the Youganwo Fm, faster  
16 than or similar to those in N1, i.e., the Huangniuling Fm; c, the correlation leads to the drastic  
17 difference in sedimentation rates between the upper (R2) and lower (N2) part of the studied  
18 Youganwo Fm; d, the sedimentation rates for the Youganwo oil shale are too fast in  
19 comparison to those of well-dated organic-rich shales in deep-time; e, the sedimentation rates  
20 of the Youganwo oil shale are compatible with those of well-dated organic-rich shales in  
21 deep-time and the sedimentary cycles in both Huangniuling Fm (N1) and the Youganwo Fm  
22 (R2 and N2) are in the orbital frequency bands and likely represent eccentricity cycles.

23

#### 24 **Figure captions**

25 **Figure 1** Location and regional geology of the study area. (a) Map showing the location of  
26 the Maoming Basin, Guangdong Province, southern China. (b) Simplified geological map of  
27 the Maoming Basin. 1. Precambrian; 2. Upper Cretaceous; 3. Youganwo Fm.; 4.  
28 Huangniuling Fm.; 5. Shangcun Fm.; 6. Laohuling Fm.; 7. Gaopengling Fm.; 8. Quaternary; 9.  
29 Fault; 10. Investigated Jintang section. MR, MB, and MS mark the sites where samples were  
30 collected for a magnetostratigraphic study by Wang et al. (1994). See text for details.

1 **Figure 2** Stratigraphy of the investigated section exposed in the now abandoned open mine  
2 pit in the Maoming Basin. Lithostratigraphic column (a) shows that the investigated section  
3 contains the Youganwo Fm and the overlying Huangniuling Fm. The stratigraphic column of  
4 the upper part of the Huangniuling Fm schematically shows the overall rhythmic sedimentary  
5 feature that is characterized by the repeated occurrence of a sedimentary package that is  
6 composed of a thin bed (shown in red lines) of red sandstone at the base, massive grey  
7 sandstone in the middle, and a light grey mudstone bed at the top. The Youganwo Fm also  
8 exhibits sedimentary rhythms that are characterized by repeated occurrence of the beds with  
9 distinct reddish color (shown in pinkish lines) at distance. Sedimentary cycles (b) are reflected  
10 by magnetic susceptibility data. The distinct reddish beds in the Youganwo Fm and the thin  
11 red sandstone layers in the Huangniuling Fm generally correspond to the magnetic  
12 susceptibility peaks. The distinct thin red sandstone layer of a sedimentary package in the  
13 Huangniuling Fm is numbered and a total of 19 sedimentary packages are identified. Note the  
14 different scales of the magnetic susceptibility of the Youganwo Fm (the lower part) and the  
15 Huangniuling Fm (the upper part). Field photographs (c-e) show the major sedimentary  
16 features of the two formations and the contact between them. In (c), the red arrows indicate  
17 the red, thin marker bed of sandstone in the Huangniuling Fm. In (d), the arrow marks the  
18 contact between the two formations, displaying a continuous, gradual transition from brown  
19 grey mudstones at the uppermost of the Youganwo Fm to pale grey mudstones at the base of  
20 the Huangniuling Fm. In (e), the yellow ellipse at the lower-middle part of the picture marks a  
21 person (~1.6 m) for scale; red arrows point to several distinctive reddish layers that form the  
22 sedimentary rhythms in the Youganwo Fm. br grey = brown grey, lt grey = light grey.

23 **Figure 3** Spectral analysis of the depth series of magnetic susceptibility data of the  
24 Youganwo oil shale. The analysis reveals dominant sedimentary cycles with cycle wavelength  
25 ratios similar to periodicity ratios of orbital cycles, suggesting that these sedimentary cycles  
26 probably represent orbital cycles. The red curve represents the noise level above which the  
27 spectral peaks are considered statistically significant. The numbers above the spectral peaks  
28 indicate cycle wavelength (in cm) of the sedimentary cycles. See text for details.

29 **Figure 4** Anisotropy of magnetic susceptibility (AMS) data of the Youganwanwo Fm (a, b)  
30 and the Huangniuling Fm (c, d).  $k_1$ ,  $k_2$ ,  $k_3$  are the maximum, intermediate, and minimum  
31 axis of the anisotropy ellipsoid, respectively. (a, c) are the equal area projection of these



1 principal axes. No. is the number of specimens. T and Pj in (b, d) are the shape factor and the  
2 degree of anisotropy, respectively (Jelinek, 1981).

3 **Figure 5** Rock magnetic data of samples from the Youganwo Fm and Huangniuling Fm. (a) –  
4 (e), temperature dependence of magnetic susceptibility (MS) of samples from the  
5 Huangniuling mudstone (a, b), the uppermost brown grey shale (c) and the oil shale (d, e) of  
6 the Youganwo Fm during a heating-cooling cycle between room temperature and 700°C; (f),  
7 IRM acquisition and the subsequent demagnetization in a backward DC field; (g-j), Zero-  
8 field-cooled (ZFC) and field-cooled (FC) low temperature measurements of the representative  
9 samples. The arrow in (g) marks the subdued Verwey transition; (k-o) thermal  
10 demagnetization of the composite IRM that was acquired along Z-, Y-, and X-axis at a field  
11 of 1.2T, 0.6T, and 0.125T, respectively.

12 **Figure 6** Representative demagnetization data of samples from the studied section.  
13 Open/closed squares indicate the vertical/horizontal components.

14 **Figure 7** Characteristic remanent magnetization in stratigraphic coordinates. The solid/open  
15 symbols represent the lower/upper hemisphere projection.

16 **Figure 8** Integrated litho-, cyclo-, and magnetostratigraphy (a-f) of the investigated section,  
17 and the correlation with the  $\delta^{18}\text{O}$  and  $\delta^{13}\text{C}$  records (g, h) from the equatorial Pacific deep-sea  
18 sediments (ODP site 1218) (Pälike et al., 2006) as well as the chrono- and lithostratigraphy (i)  
19 of Massignano section in Italy (the Eocene-Oligocene boundary global stratotype section and  
20 points, GSSP) (Jovane et al., 2009), showing the Eocene-Oligocene climatic transition (EOT)  
21 and its precursor events. The legends for lithology and sedimentary cycles of the studied  
22 section in the Maoming Basin are the same as those in Fig. 2. In (c, d), the solid (open)  
23 symbols represent “A”(“B”)-quality ChRM data. Note that major lithological change from the  
24 Scaglia Variegata Fm to the Scaglia Cinerea Fm occurs at 12 m, which corresponds to the  
25 early stage of Chron C13r (i), while the major lithological change at the investigated section  
26 occurs at the late stage of Chron C13r (a, f).

27

**Table 1 Correlations of magnetozones with Chrons C18 to C13 of the geomagnetic polarity timescale (GPTS)**

		Polarity Chrons/subchrons (duration in myr)														
Correlations	Polarity zone*	<b>C18n</b> (1.529)	C18r (1.01)	<b>C17n</b> (1.363)	C17r (0.283)	<b>C16n.2n</b> (0.649)	C16r (0.269)	<b>C16n.1n</b> (0.186)	C16n.1r (0.159)	<b>C16n.2n</b> (0.649)	<b>C15n</b> (0.295)	C15r (0.411)	<b>C16n</b> (0.994)	<b>C13n</b> (0.548)	C13r (1.294)	<b>C15n-C17n</b> (3.334)
1	<b>N1</b>	<b>1.23, 382</b>	-													
	x <sup>a</sup> R2	-	0.71, 337													
2	<b>N1</b>			<b>1.38, 341</b>	-											
	x <sup>b</sup> R2			-	2.54, 94											
3	<b>N1</b>					<b>2.90, 162</b>	-									
	x <sup>b</sup> R2					-	2.68, 90									
4	<b>N1</b>							<b>10.11, 47</b>	-	-						
	R2							-	4.53, 53	-						
	x <sup>c</sup> <b>N2</b>							-	-	<b>2.31, 76</b>						
5	<b>N1</b>										<b>6.37, 74</b>	-	-			
	R2										-	1.75, 137	-			
	x <sup>d</sup> <b>N2</b>										-	-	<b>1.51, 117</b>			
6	<b>N1</b>													<b>3.43, 137</b>	-	-
	R2													-	0.56, 431	-
	√ <sup>e</sup> <b>N2</b>													-	-	<b>0.42, 392</b>

Note: \*, N1 is defined from 32.2 to 51.0 m and contains ~ 4 sedimentary cycles; R2 is defined from 25.0 to 32.2 m and contains ~3 sedimentary cycles; N2 is defined from 11.0 to 25.0 m and contains ~8.5 sedimentary cycles. Bold (regular) fonts indicate normal (reversed) polarity zones/chrons; The two numbers in each cell are sedimentation rate in cm/kyr and the periodicity of the sedimentary cycle (in kyr) calculated based on the correlation. For example, 1.23, 382 in the very first cell indicate that the sedimentation rate is 1.23 cm/kyr and the sedimentary cycle represents 382 kyr based on Correlation 1. "-" denotes "not applicable"; "x" indicates that the correlation is unrealistic and is rejected. "√" indicates acceptable correlations; a-e provide brief comments on why a correlation is rejected or accepted. a, the correlation would place the majority of the Youganwo Fm, i.e., N2-N3, to the Middle Eocene; b, the correlation would result in sedimentation rates in R2, i.e., the Youganwof Fm, faster than or similar to those in N1, i.e., the Huangniuling Fm; c, the correlation leads to the drastic difference in sedimentation rates between the upper (R2) and lower (N2) part of the studied Youganwo Fm; d, the sedimentation rates for the Youganwo oil shale are too fast in comparison to those of well-dated organic-rich shales in deep-time; e, the sedimentation rates of the Youganwo oil shale are compatible with those of well-dated organic-rich shales in deep-time and the sedimentary cycles in both Huangniuling Fm (N1) and the Youganwan Fm (R2 and N2) are in the orbital frequency bands and likely represent eccentricity cycles.

Fig. 1

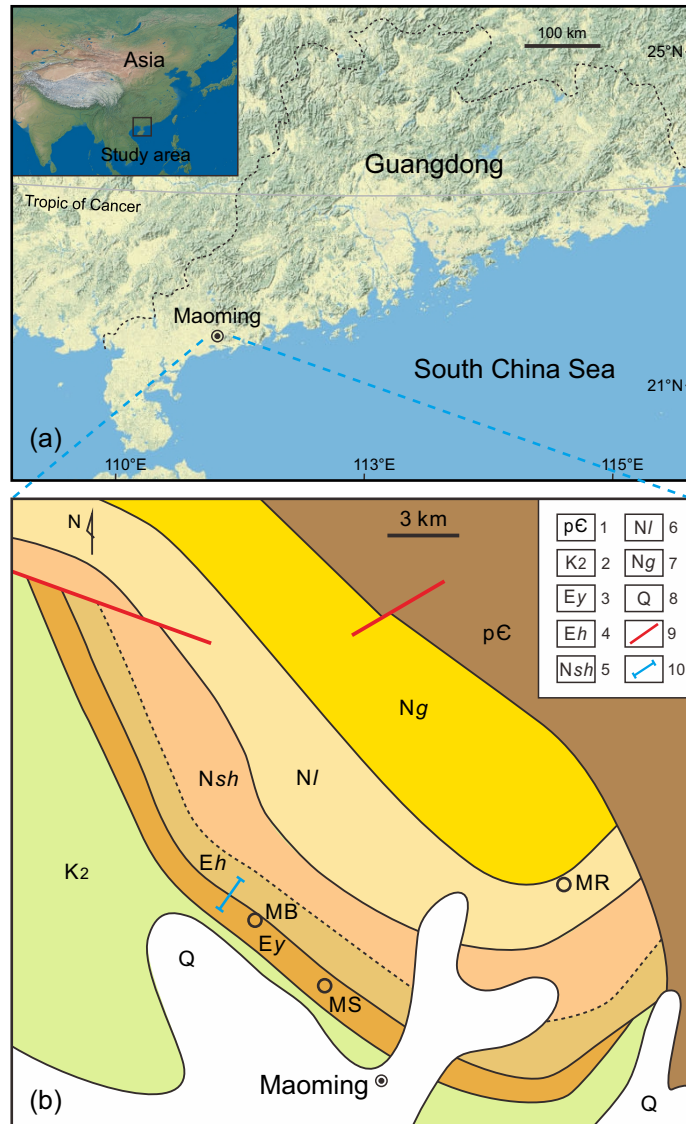


Fig. 2

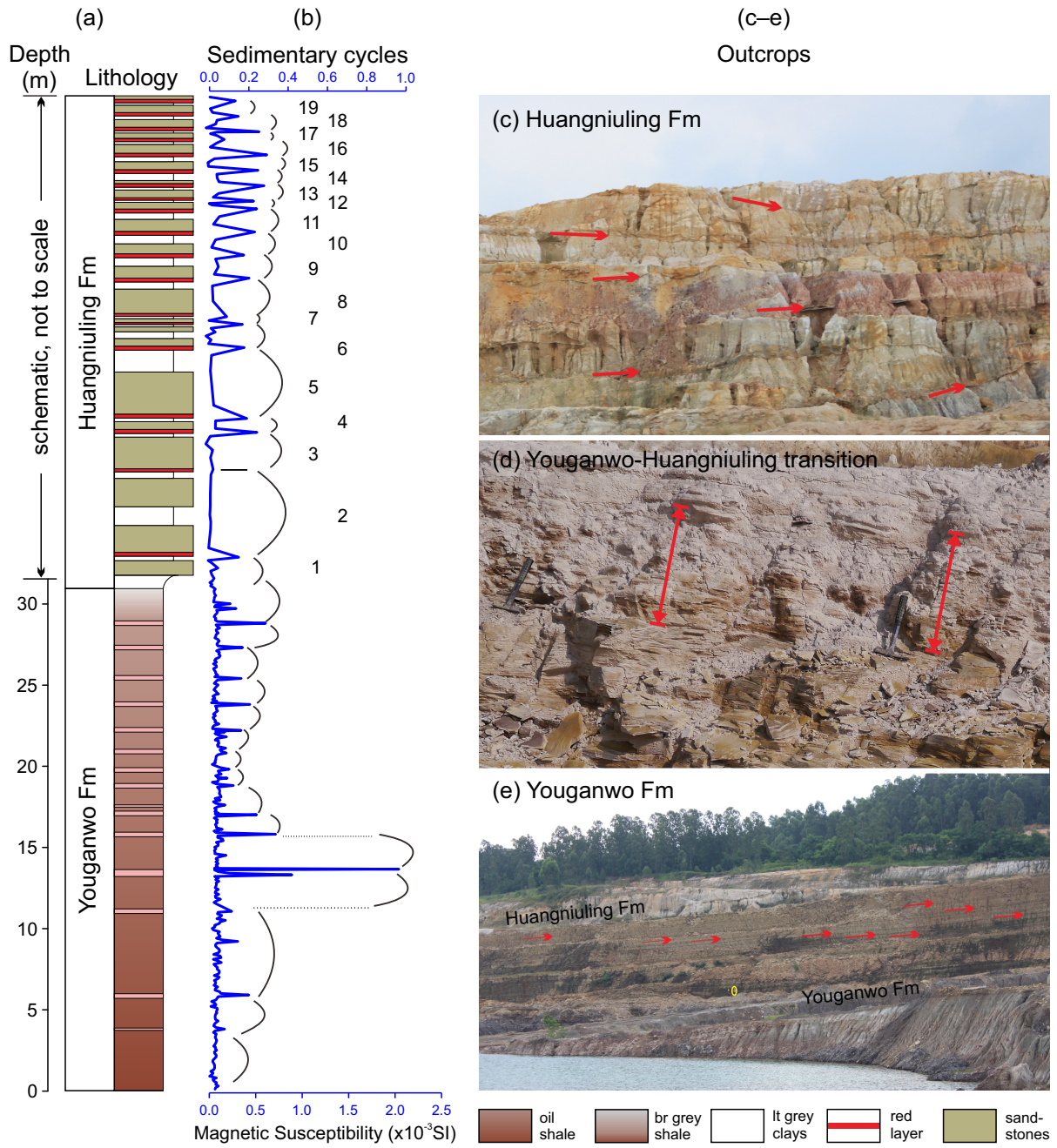


Fig. 3

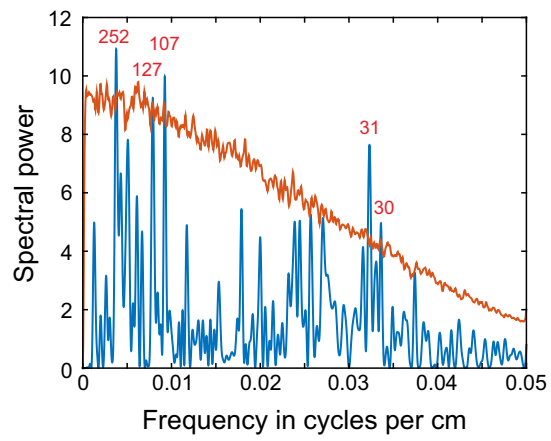


Fig. 4

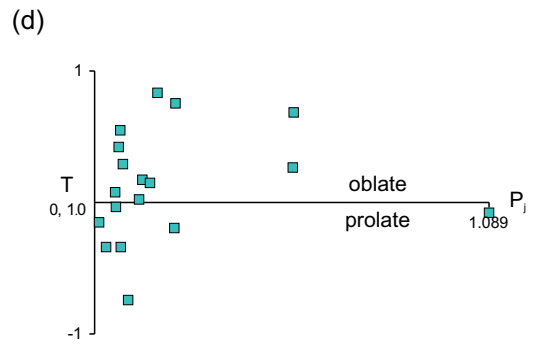
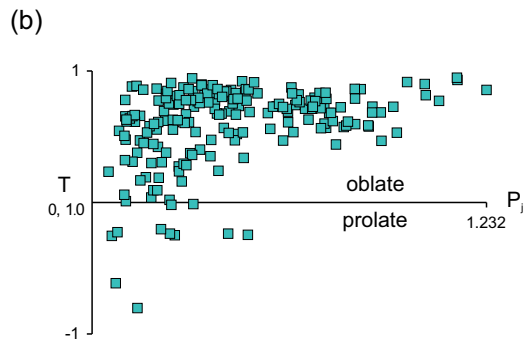
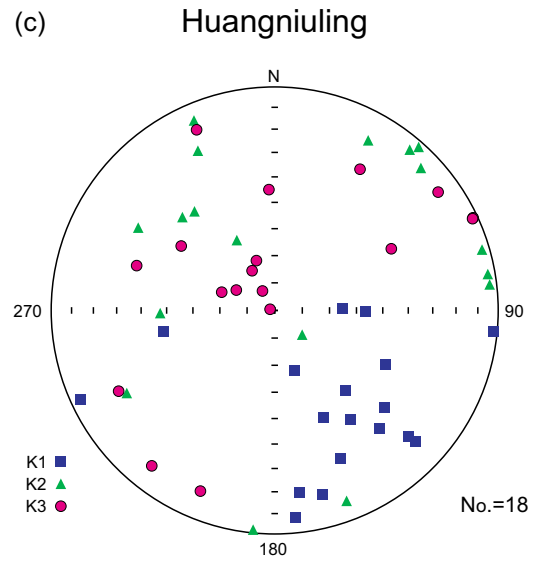
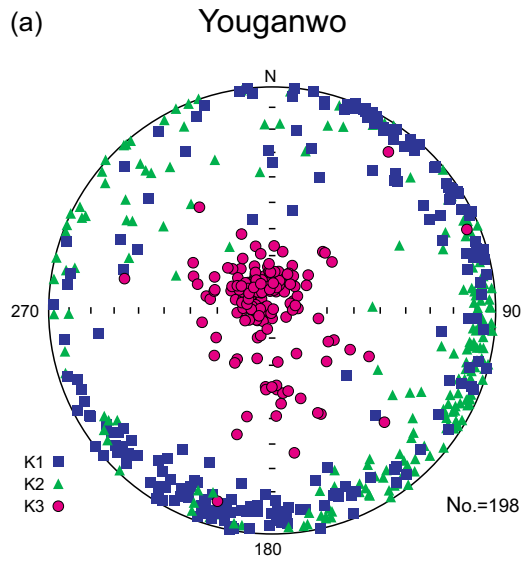


Fig. 5

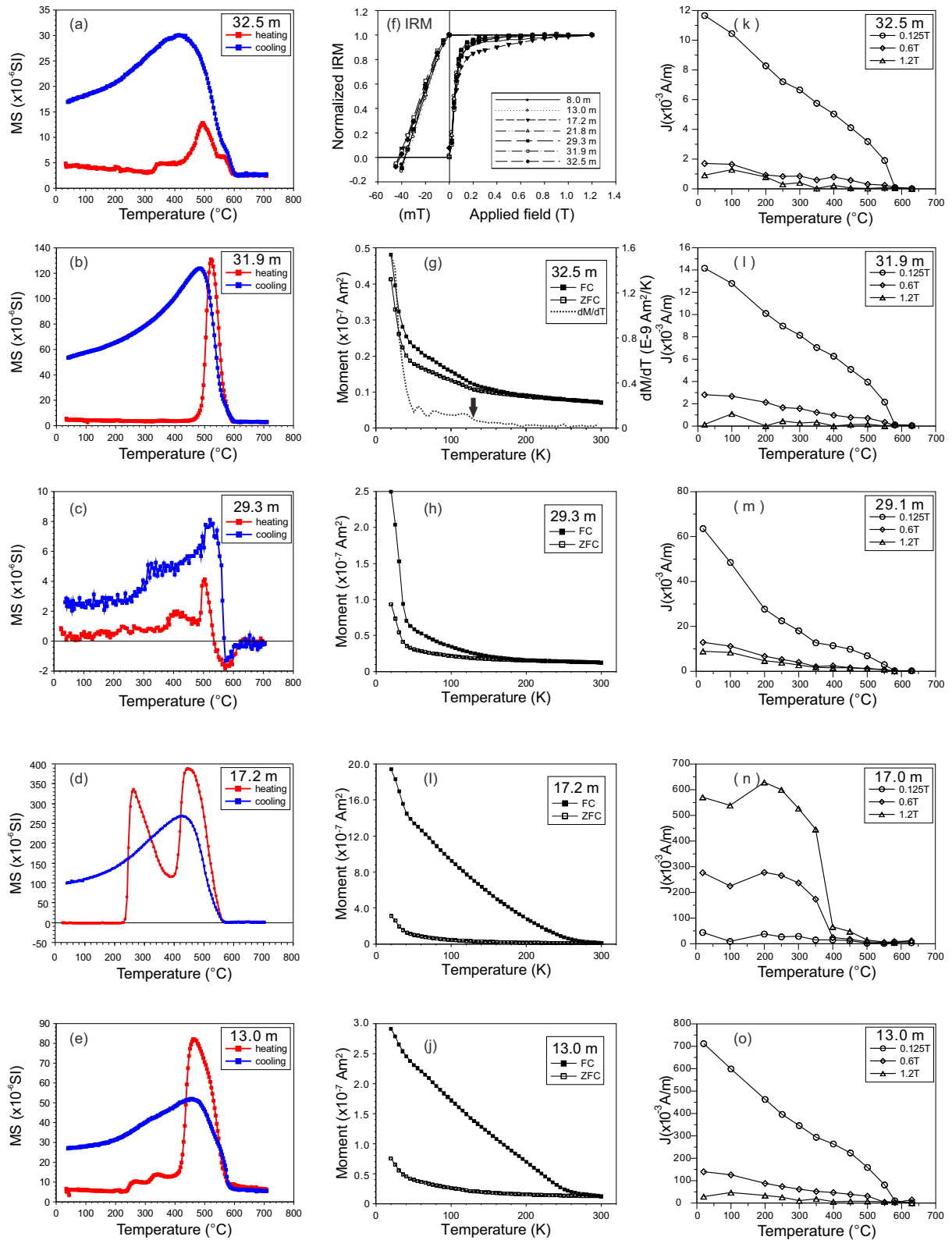


Fig. 6

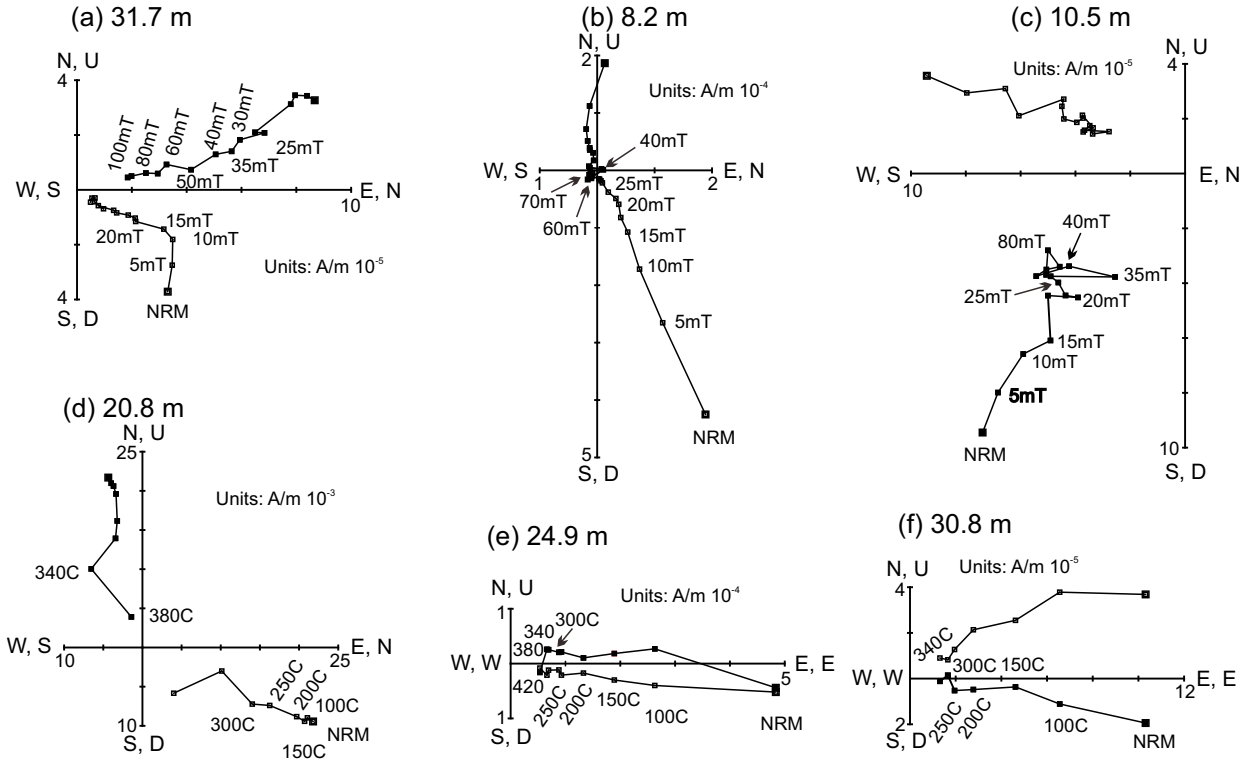




Fig. 7

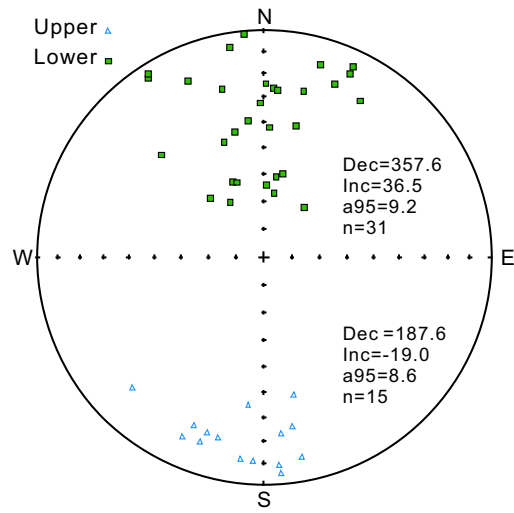


Fig. 8

